Nanoscale Horizons

ROYAL SOCIETY OF CHEMISTRY

REVIEW

View Article Online
View Journal

Cite this: DOI: 10.1039/d5nh00390c

Powering the future: advances, challenges, and sustainability of polymer electrolytes in lithium–sulfur batteries

Dipsikha Ganguly, Rayavarapu Prasada Rao and Seeram Ramakrishna *

Received 3rd June 2025,
Accepted 17th September 2025

DOI: 10.1039/d5nh00390c

rsc.li/nanoscale-horizons

Lithium–sulfur (Li–S) batteries offer a transformative theoretical energy density (~2600 Wh kg^{-1}), positioning them as strong candidates for next-generation energy storage systems supporting the global shift toward renewable energy integration and electrified transportation. However, their commercial viability is hindered by challenges such as the polysulfide shuttle effect and safety concerns related to volatile liquid electrolytes. Polymer-based solid-state electrolytes present a compelling pathway to overcome these barriers, offering improved safety, processability, and design flexibility. This review critically examines recent advancements in polymer electrolytes for Li–S batteries, with a particular focus on nanoscale strategies to enhance ionic conductivity, electrochemical stability, and electrode–electrolyte interfacial compatibility. Special attention is paid to nanostructured polymer matrices, functional nanofillers, and interfacial engineering techniques. This review also explores emerging directions, including the development of adaptive "smart" electrolytes and the integration of machine learning for rational materials design. Finally, the environmental and sustainability profiles of polymer-based Li–S batteries are compared with those of conventional lithium-ion systems, considering life cycle aspects such as raw material sourcing, fabrication energy intensity, and global warming potential. This review aims to bridge the gap between nanoscale innovation and macroscopic energy challenges, highlighting the potential of polymer electrolytes to enable scalable, safe, and sustainable Li–S battery technologies.

1. Introduction

The widespread impact of lithium-ion batteries (LIBs) is evident in their pervasiveness across a plethora of daily life aspects, from mobility applications to grid-scale energy storage.[1,2] The United Nation (UN) sustainable development goals (*e.g.* (7) affordable clean energy, (11) sustainable cities and communities and (13) climate action) also act as a catalyst in accelerating battery development. However, despite this success story, there are limitations that restrict their adoption for more challenging applications. Two of the important limitations are the safety and environmental impact of liquid lithium batteries. The United Nations Sustainable Development Goals (SDGs) call for greater use of clean energy, but conventional lithium-ion batteries (LIBs), which use flammable liquid electrolytes, pose a significant risk of thermal runaway, fire, and explosion.[3] Another limitation of LIBs is their low theoretical energy density; while current research and developments suggest significant improvements over previous battery technologies; the theoretical energy density still has a limit of around 350 Wh kg^{-1}.[4,5] This engenders the need to transition to high energy density battery chemistries, for EVs and grid energy storage.[5] In the pursuit of safer and high energy density solutions, Li–S batteries have emerged as a promising opportunity.[6,7] Lithium sulfur batteries possess a significantly higher (nearly sevenfold increase) energy density of ~2600 Wh kg^{-1} compared to conventional Li-ion batteries.[8] This capacity directly enables substantially longer driving ranges for EVs and facilitates lighter, more compact designs for both portable electronics and grid storage applications. Additionally, sulfur, the key cathode component of Li–S batteries, is abundant in nature and relatively inexpensive compared to the materials used in LIB cathodes.[9] This combination of high energy output, economic viability, and sustainable design makes them a highly attractive option for future energy storage applications. The global battery market is booming, fuelled by the surging demand for EVs, renewable energy integration, and long-lasting portable devices. Analysis predicts that the Li-ion battery market will reach $1 trillion by 2030.[10,11] This market clearly needs high-performance safer batteries with increased energy density. Solid-state Li–S batteries, with their unique combination of these features, present a

Department of Mechanical Engineering, College of Design and Engineering, National University of Singapore, 9 Engineering Drive 1, Singapore, 117575, Singapore. E-mail: seeram@nus.edu.sg

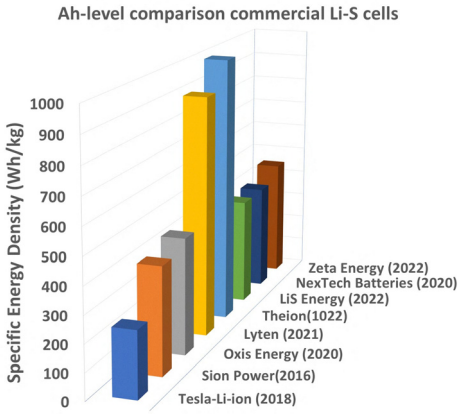

Fig. 1 Commercial and research-based energy density (Ah) targets (300–600 Wh kg^{-1} of LSB pouch cells, reproduced from the data and news reports[12–15,17]).

persuasive solution compared to existing LIB technology. Zhou *et al.* demonstrated the commercial and research-based energy density (Ah) targets (300–600 Wh kg^{-1}) for LSB pouch cells (Fig. 1), which are better than the existing Li-ion cylindrical cells (246 Wh kg^{-1}) used by Tesla-Model 3 electric cars.[12–16] Also, the Ah-level commercial data clearly direct that Li–S will be a real trailblazer in the electric vehicle industry.

Lyten has fast-tracked its timeline with a 3D graphene-based material as a sulfur host for cathodes to produce Li–S cells. Lyten has raised over $625 million in total equity investment, which includes a $200 million Series B round led by Prime Movers Lab in September 2023. Additionally, the company has a letter of intent for a $650 million loan from the U.S. Export-Import Bank.[17] LiS energy is currently positioning itself as a semi-solid Li–S battery manufacturer and anticipated its Gen-3 technology with a gravimetric capacity of 400 Wh kg^{-1} and a volumetric capacity of 540 Wh L^{-1}.[13] However, their R&D is also focusing on full-solid-state batteries through collaborative research at Deakin University. Battery reports 2022[18] shows the funding, patent portfolio and chemistries of existing Li–S battery companies (Fig. 2).

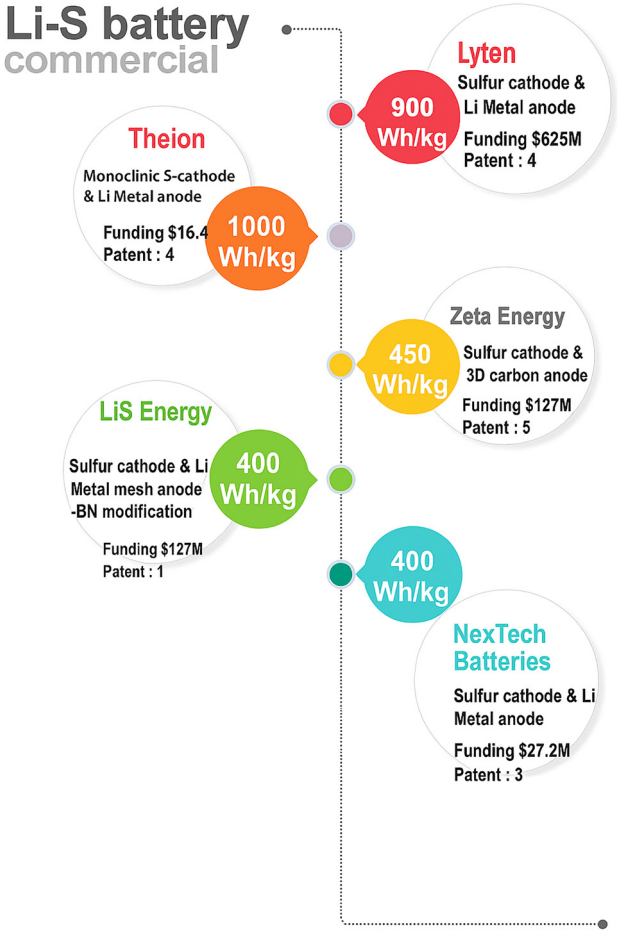

Fig. 2 Commercial energy density targets from existing Li–S companies (drawn based on the data of ref. 18 and news reports).

1.1. Limitations of liquid Li–S batteries

Although lithium–sulfur (Li–S) batteries exhibit promising features, they face considerable challenges in achieving commercialization. The process of converting elemental sulfur (S_8) to lithium sulfide (Li_2S) involves a series of multi-step reduction reactions (eqn (1)–(4) and Fig. 3b). During the discharge process, higher-order lithium polysulfides (Li_2S_n, where $8 \leq n \leq 3$) are generated as sulfur interacts with lithium ions in the liquid electrolyte. Subsequently, these highly soluble polysulfides are transformed into lower-order, insoluble polysulfides (Li_2S_2/Li_2S), as illustrated in Fig. 3(a and b).

$$S_8 + 2Li^+ + 2e^- \rightarrow Li_2S_8 \quad (1)$$

$$Li_2S_8 + 2Li^+ + 2e^- \rightarrow 8Li_2S_4 \quad (2)$$

$$2Li_2S_4 + 4Li^+ + 4e^- \rightarrow 4Li_2S_2 \quad (3)$$

$$4Li_2S_2 + 8Li^+ + 8e^- \rightarrow 8Li_2S \quad (4)$$

Fig. 3c clearly shows the issues hindering the progress of Li–S technology. During the cycling, the polysulfides accumulated at the anode physically block the coverage of the active sites, resulting in inefficient transfer of lithium ions and degradation in the battery performance. Second, the shuttle effect, where the soluble higher order polysulfide shuttles between the anode and cathode at discharge, eventually reduces the shelf life and lifespan of the battery.[8,20] Finally, the Li-metal anode commonly used in Li–S batteries is susceptible to reaction with the polysulfides, forming lithium sulfide (Li_2S) – a non-conductive and non-electrochemically active species. These further compromise the battery efficiency.[21]

1.2. Solid-state polymer electrolytes

To curb the issues of shuttle effects and polysulfide blocking, solid-state Li–S batteries represent a promising technological advancement.[22] These batteries transform next-generation battery technology by substituting liquid electrolytes with solid ones, solid state batteries (SSBs). Solid electrolytes provide numerous benefits, such as improved safety due to their non-

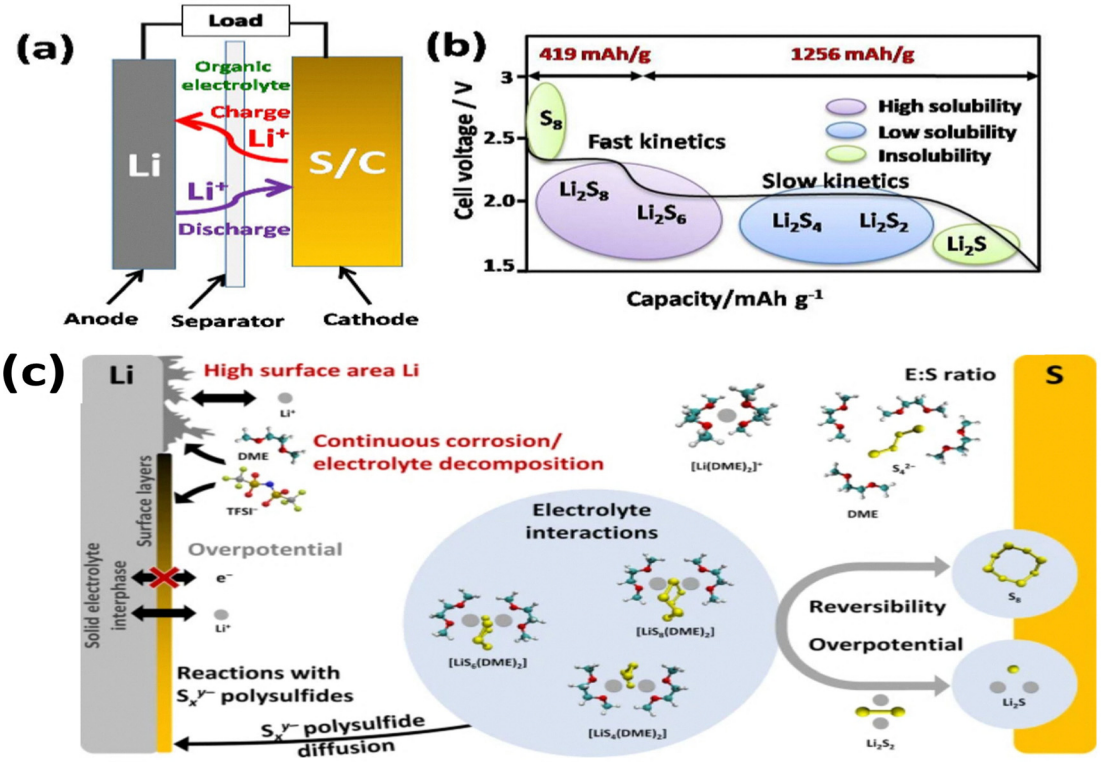

Fig. 3 (a) Working principle, (b) polysulfide species formation in different operational voltage ranges and (c) degradation mechanisms of Li–S batteries (molecular structure: ref. 19). This figure has been adapted/reproduced from ref. 19 with permission from Wiley copyright 2021.

flammability and the ability to suppress the polysulfide shuttle effect by physically hindering the diffusion of polysulfides within the battery.[23] However, solid-state batteries currently face challenges with brittleness and interfacial stability at the electrode–electrolyte interface. This brittleness can lead to mechanical failure during battery operation, while poor interfacial stability can hinder ionic conductivity and battery performance.[23–25] The constraints of SSBs have led to increased demand in polymer electrolytes for Li–S batteries, due to significant advantages. Polymer electrolytes offer a hybrid approach that combines the advantages of solid and liquid electrolytes, providing interfacial compatibility and flexibility.[26–28] They offer the safety benefits and potential for improving interfacial stability of solid electrolytes while maintaining some of the flexibility and processability of liquid electrolytes (Fig. 4).[26]

Polymer electrolytes offer several advantages over conventional liquid electrolytes that make them particularly promising for Li–S batteries.[27,29,30] Fig. 5 shows web of science estimation of patents and literature on ''polymer in Li–S batteries'' as of 2025 and Pie chart distribution of polymer electrolytes, cathodes and binders for Li–S batteries.

Polymer-based electrolytes offer a significant advantage over their liquid counterparts and inorganic solid electrolytes in Li–S batteries.[30]

1.2.1. Improved safety. Polymers are non-flammable, which significantly reduces the risk of thermal runaway and ensures the safety/durability of traditional batteries, a major problem with liquid electrolytes.

1.2.2. Good mechanical properties. The polymeric backbone offers the potential to enhance the mechanical stability of solid state Li–S batteries. In comparison with brittle solid electrolytes, polymer electrolytes can exhibit a degree of flexibility,[31] which helps in eliminating mechanical failure during high charge rates due to rapid volume changes. This flexibility also helps in achieving better interfacial stability of the electrolyte–electrode interphase, resulting in superior battery performance and lifespan.[32]

1.2.3. Tailorable design for selective ion transport. One of the main advantages of polymer electrolytes is their tunability. Polymer electrolytes can be modified by carefully choosing and modifying the polymer backbone and incorporating suitable additives helping in lithium ion transport.[33,34] Fig. 6 shows various strategies to achieve selective ion transport.[35]

1.2.4. Ionic conductivity enhancement. The incorporation of different salt dopants or functional groups into the polymer matrix can improve the lithium-ion migration in electrolytes thus improving battery performance. Table 4 shows the effect of different polymer backbones and their mechanical strength and ionic conductivity on lithium metal battery stability.

1.2.4.1. Polar group incorporation. Incorporating polar groups into a base material achieves two crucial goals: it enhances lithium-ion interaction through increased polarity

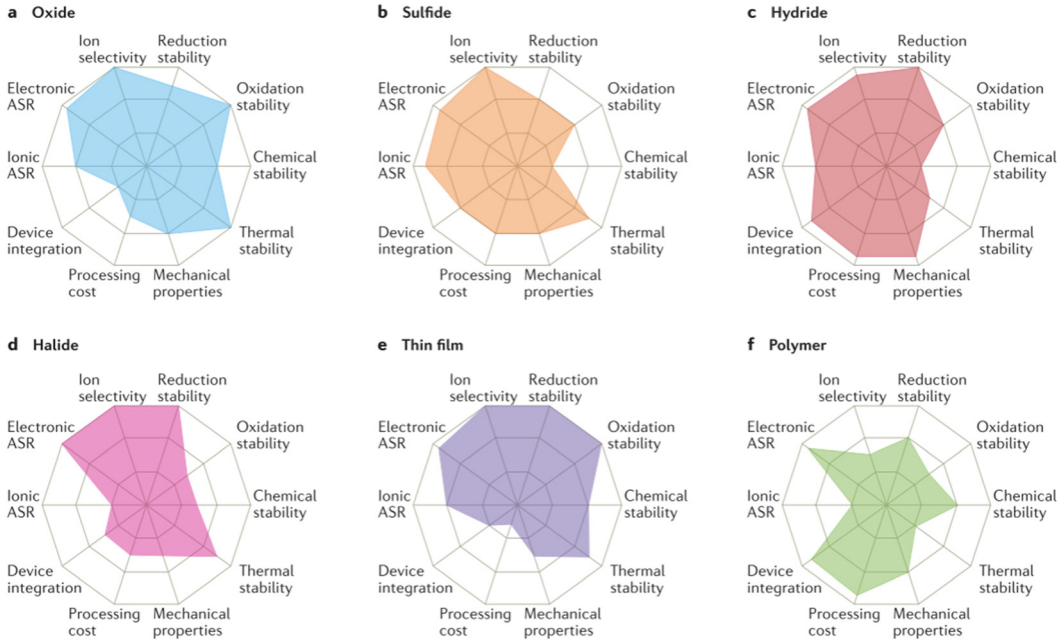

Fig. 4 Properties of different solid-state electrolytes. This Fig. 4(a–f) has been reproduced from ref. 26 with permission from Springer Nature copyright 2017.

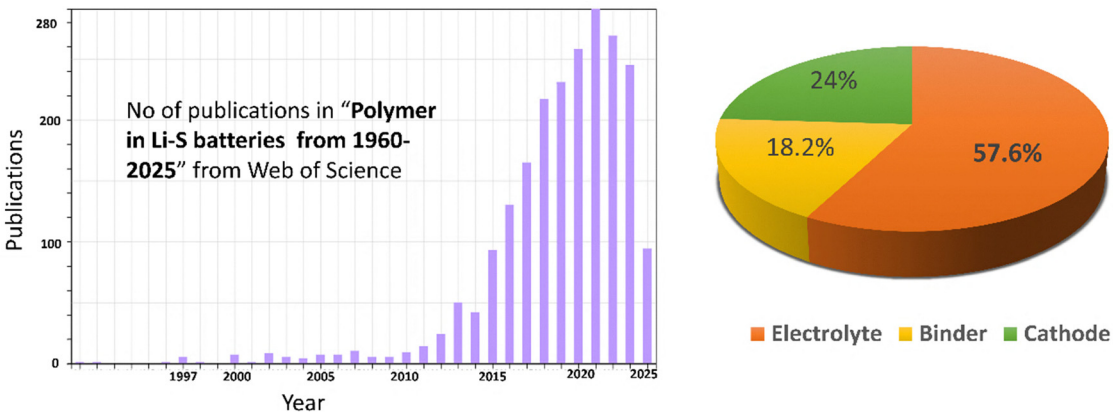

Fig. 5 Works on "polymer in Li–S batteries" (1960–2025) and Pie chart distribution of polymers (electrolytes, cathodes and binders).

and simultaneously restricts the diffusion of larger, undesirable molecules like polysulfides.

1.2.4.2. Crosslinking. Crosslinking the polymer chains can create stronger networks that may form in a polymer, hence leading to improved mechanical strength and probably reduced sulfur diffusion across molten salts.

1.2.4.3. Suppression of polysulfide dissolution. Polymer electrolytes possibly mitigate the dissolution of polysulfides. The polymeric matrix helps in blocking the dissolution of polysulfides in electrolytes and subsequent interaction.[36] Additionally, specific functional groups and fillers incorporated into the polymer matrix can interact with polysulfides by chemical interaction or surface adsorption, helping in better confinement and conversion.

1.3. Market drivers and industry trends

The Li–S battery market is set to experience considerable growth driven by the increasing need for high-performance energy storage solutions.[10,12] Several key factors drive this growth.

1.3.1. Increasing demand for EVs and renewable energy integration. The rising popularity of electric vehicles and the growing importance of solar energy, wind energy, geothermal energy and other different forms of renewable energies require better energy storage. These demands can be fulfilled by Li–S batteries considering their higher theoretical capacities than any other existing technologies, thus potentially increasing the

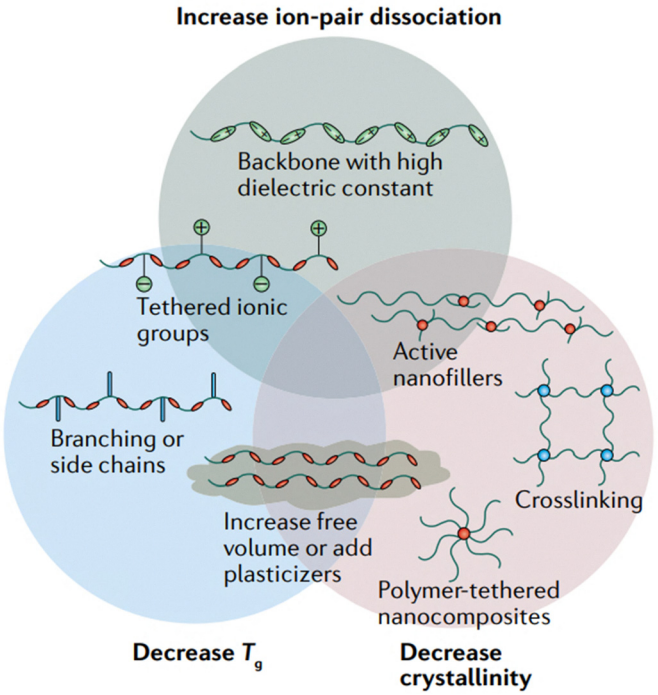

Fig. 6 Approaches to increase the ionic conductivity of polymer electrolytes. This figure has been reproduced from ref. 19 with permission from Springer Nature copyright 2025.

mileage and range of EV for enabling large scale grid integration.[12]

1.3.2. Investments and initiatives. Governments across the globe are realizing the potential benefits accrued from Li–S batteries, thus investing in research and development activities towards this end, such as China's announcement on a project worth over $830 million targeting transition to solid-state batteries illustrates the interest in emerging battery technologies.[11] This focus on battery innovation will undeniably aid the development of polymer electrolytes, as an advancement in solid-state electrolyte research can provide valuable insights for polymer electrolyte design. Industry consortiums like China All-Solid-State Battery Collaborative Innovation Platform (CASIP) further emphasize the importance of developing next-generation batteries.[10,37] CASIP, with its involvement from leading battery manufacturers, electric vehicle manufacturers, and research institutions, proposes to build a robust supply chain by 2030 for solid-state batteries. The initial focus will be on solid-state Li-batteries with probable advancements in polymer electrolytes for improving battery performance.[38]

1.4. Challenges with polymer electrolytes for Li–S batteries

The Li–S battery market is anticipated to witness a significant growth in the near-term future for high-performance and long-lasting high energy density storage solutions. Polymer electrolytes will be one of the major advancements.[30,39] However, polymer electrolytes also possess some hurdles to overcome in accelerating the commercialization of Li–S batteries.

1.4.1. Ionic conductivity *vs.* mechanical properties. Balancing between ionic conductivity (σ) and mechanical strength is a crucial challenge.[26] While some polymer electrolytes demonstrate impressive ionic conductivity, their mechanical properties might be insufficient for practical applications.

1.4.2. Long-term stability. Ensuring reliable battery performance through the long-term stability of polymer electrolytes is important. Chemical and electrochemical degradation during charge–discharge cycles may cause deterioration in the characteristics of the electrolyte over time. Research efforts are focused on developing stable polymer electrolytes incorporating additives as fillers or backbone modifications.[27,39]

1.4.3. Interface compatibility. Efficient ion transport and good battery performance require maintaining good interfacial compatibility. However, differences in the chemical and physical properties between the electrodes and the electrolyte could create interfacial resistance that hampers ion transfer. To improve interfacial compatibility, different strategies like surface modification of electrodes or tailoring the polymer electrolyte were reported.[40]

This review article explores the current cutting edge research in polymer electrolytes for Li–S batteries, highlighting the challenges and opportunities in this field. This review also delves deeper into the Li-ion conduction mechanism of polymer electrolytes, through molecular dynamics simulations and experimental validation. This review also talks about some recent developments in self-healing polymer electrolytes for smart futuristic Li–S batteries. Finally, this review discusses the environmental impact of solid state Li–S batteries, future directions, and potential breakthroughs achieved using

artificial intelligence and machine learning that could pave the way for the widespread adoption with the aid of advanced polymer electrolytes in the commercial market.

2. Progress in polymer electrolytes

Polymer electrolytes can be classified into three main types: (a) solvent free or solid or polymer electrolytes (SPEs) (b) gel polymer electrolytes (GPEs) and (c) composite polymer electrolytes (CPEs). Fig. 7 shows the schematic depiction of the different types of electrolytes used in Li–S batteries.

SPEs consist of a solid polymer matrix which facilitates lithium ion transport. It offers exceptional safety because of the absence of flammable liquids. Polyethylene oxide (PEO) is the most widely used SPE backbone for Li–S batteries,[41] however its low ionic conductivity at room-temperature can limit the performance. Advancements in polymer design and the incorporation of conductive additives are being carried out to address this challenge. GPEs are a combination of SPEs and liquid electrolytes.[36] GPEs can achieve comparatively higher ionic conductivity than SPEs, and good interfacial compatibility. However, in GPEs, incorporation of liquid plasticizers results in lower mechanical stability and less safety. To address the limitations of both SPEs and GPEs, CPEs have been developed. These comprise different fillers incorporated within the polymer matrix. Moreover, specific fillers can be included for dealing with specific problems connected with Li–S batteries like trapping polysulfides or increasing electronic conductivity in the cathode. SPEs have good safety characteristics but often suffer from poor ionic conduction resulting in low lithium ion transport through the battery. CPEs adopt both approaches by infusing ceramics or nanoparticles into the polymeric material. Due to their ability to enhance ionic conductivity, these additives such as ceramic materials can increase mechanical strength. They also provide other functionalities including trapping polysulfides. Polymer electrolytes have significantly witnessed a surge of interest in recent years (Fig. 5). This is demonstrably evident in the exponential growth of published research exploring these materials, encompassing polymer electrolytes highlighted over the years in Fig. 8.

2.1. Solid polymer electrolytes (SPEs)

SPEs offer electrochemical stability, safety, and flexibility, all of which are essential for solid-state lithium-sulfur batteries. Polyethylene oxide is one of the most widely studied SPEs due to their high lithium salt solvation capabilities and film forming abilities.[23] The interaction of PEO with metal salts was first investigated by Fenton and explored by Armand.[42] Studies showed that at elevated temperatures, molten PEO exhibits liquid-like behavior, leading to a phenomenon like the polysulfide shuttle effect observed in ether-based electrolyte solvents.[43] The strong attraction between PEO and Li_2S_n (n = 1–8), as evidenced by the elevated Gutmann Donor Numbers of ethylene oxide (EO) units enhances the solubility of long-chain polysulfides in PEO-based electrolytes. This phenomenon, known as the shuttle effect, has been experimentally confirmed by various research groups.[44,45] *In situ* optical microscopy is used to investigate the structural modifications and integrity of

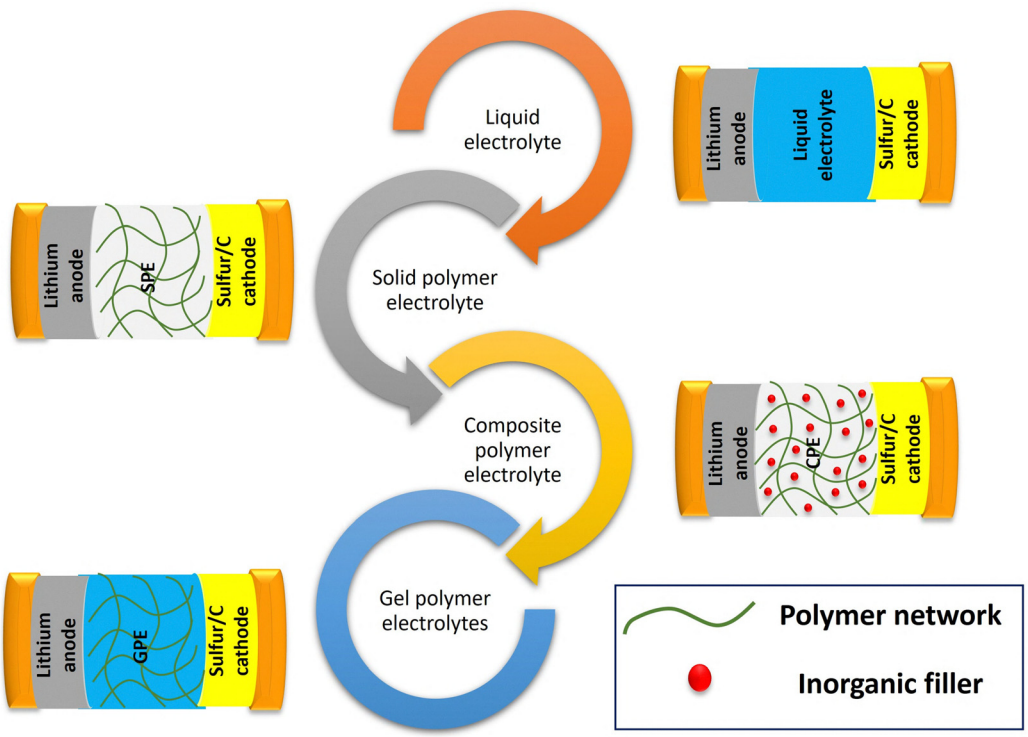

Fig. 7 Schematic depiction of liquid and polymer electrolytes in Li–S batteries.

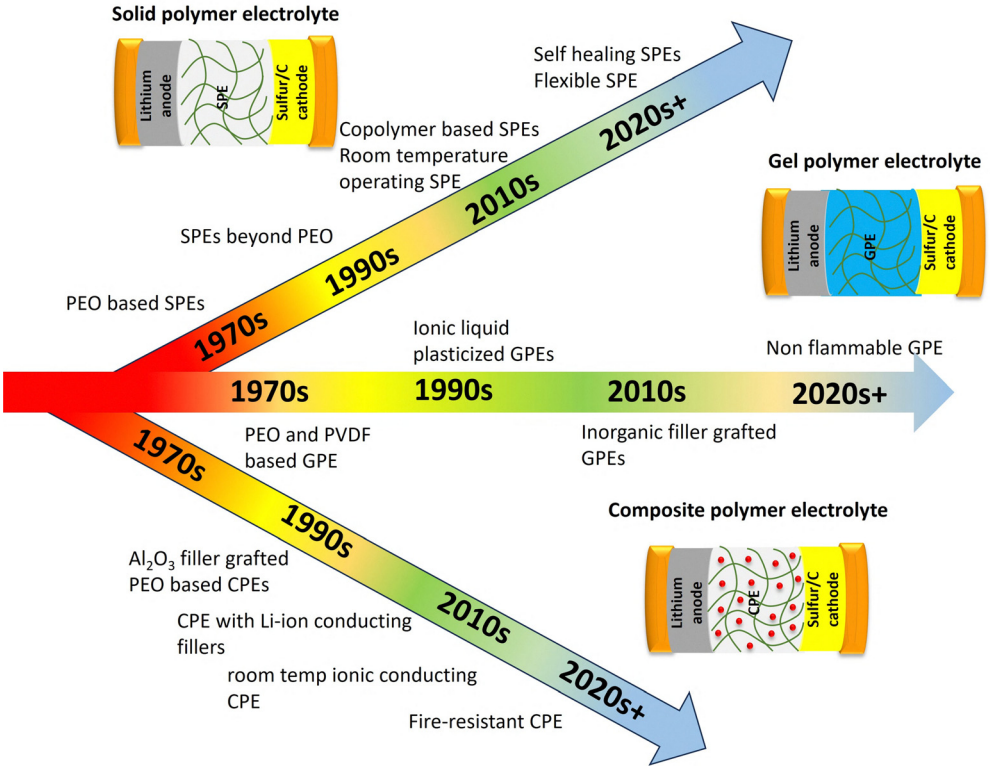

Fig. 8 A brief chronology of the development of SPEs, GPEs and CPEs over the years.

the polymer electrolyte during the discharge process confirms color change, demonstrating the dissolution of polysulfides into the PEO-based SPE, which was further investigated by Zaghib's group through *in situ* SEM imaging, and UV-Vis spectroscopy revealed the formation of S_4^{2-} polysulfides during discharge and S_6^{2-} polysulfides during charge caused the increased interfacial resistance.[46] Various techniques like infrared spectroscopy and X-ray diffraction (XRD) have been used to investigate the critical role of the electrolyte medium in addressing lithium polysulfide shuttling. The study revealed that Li_2S_8 dissolves more effectively in PEO compared to Li_2S_4. Additionally, electrochemical measurements demonstrated that PEO significantly reduces the shuttling speed of polysulfides (S_8^{2-} and S_4^{2-}) compared to conventional liquid electrolytes like 1,3-dioxolane (DOL) and 1,2-dimethoxyethane (DME). Notably, the study found that long-chain polysulfides exhibited a stronger shuttling effect than short-chain ones. These findings offer valuable insights for designing advanced SPEs for all-solid-state lithium-sulfur batteries. Further studies on the electrochemical behaviour of PEO/Li_2S_x electrolytes suggest that Li_2S_4 may partially dissociate in PEO due to its limited solubility, while Li_2S_8 tends to fully dissociate. Interestingly, PEO hinders the mobility of short-chain polysulfides (S_4^{2-}) more effectively than $TFSI^-$ anions, while Li^+ diffusion remains comparable in both systems. The higher solvation of Li_2S_8 by PEO allows for complete dissociation into Li^+ and S_8^{2-}, leading to a more conductive PEO/Li_2S_8 electrolyte compared to PEO/Li_2S_4. Meanwhile, the diffusion coefficient of S_8^{2-} (2×10^{-8} cm^2 s^{-1}) in PEO at 80 °C is slightly lower than that of S_4^{2-} (3×10^{-8} cm^2 s^{-1}), providing valuable guidance for designing SPEs to mitigate Li_2S_x transport in next-generation lithium-sulfur batteries.[47] Despite being the most widely studied SPE material, PEO faces few challenges which need to be overcome. The current trend of research focuses on improving PEO based solid state electrodes.

2.1.1. Crystallinity *vs.* amorphous phase. Major disadvantage of PEO-based SPEs is their high crystallinity at room temperature, which hinders Li-ion mobility at ambient temperatures.[48] Crystalline regions act as barriers for lithium ion transport, restricting their movement within the electrolyte.[49] Consequently, a key strategy for PEO-based SPE development involves maximizing the amorphous phase fraction. In the amorphous phase, polymer chains exhibit a more loosely packed arrangement (Fig. 9a–c), facilitating Li-ion transport and enhancing overall conductivity.[50] *Ab initio* calculations of the lithium–oxygen (Li–O) bonding environment reveal that lithium ions (Li^+) can coordinate with more oxygen atoms in amorphous than crystalline PEO. This is because the amorphous phase offers more accessible neighboring oxygen atoms. The maximum coordination number for Li^+ is 3 and 5 in crystalline and amorphous PEO, respectively. Binding energy indicates the influence of the degree of crystallinity on Li and Li^+ binding with oxygen atoms. Amorphous PEO exhibits a preference for Li^+ adsorption due to its accessible free volume and higher coordination number (Fig. 10d). This translates to an average binding energy difference of 3.36 eV/2 eV for Li/Li^+ between amorphous and crystalline PEO.[30,51]

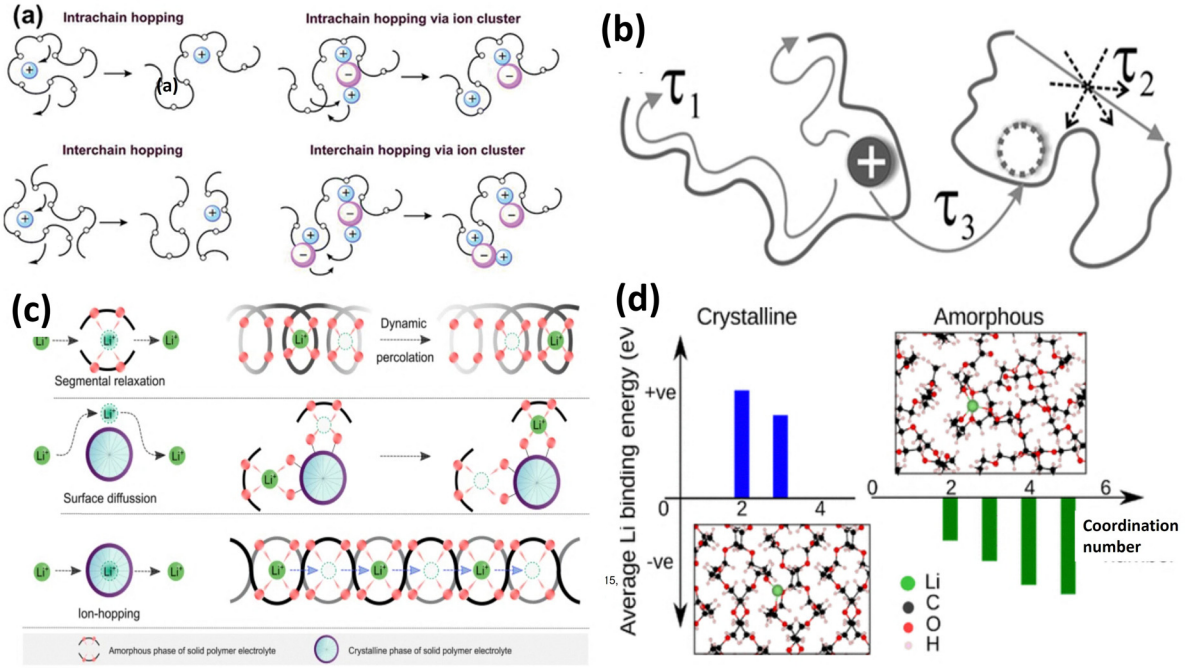

Fig. 9 Li^+ conduction in PEO, (a) in the amorphous phase. This figure has been reproduced from ref. 48 with permission from Royal Society of Chemistry copyright 2023; (b) in the amorphous and crystalline phase. This figure has been reproduced from ref. 47 with permission from American Physical Society copyright 2007; (c) ion hopping in the amorphous and crystalline state of the polymer. This figure has been reproduced from ref. 28 Springer Nature copyright 2023 and (d) molecular simulation of binding energy of Li^+/PEO. This figure has been reproduced from ref. 49 with permission from American Chemical Society copyright 2018.

2.1.2. Copolymer and functional group incorporation. Copolymerization or blending different polymers with different properties offers a good approach for SPEs. A copolymer of PEO and a highly conductive polymer like polyacrylonitrile or ester groups can leverage the good film-forming properties of PEO while benefiting from the high ionic conductivity of the copolymers.[41,54,55] However, compatibility between the co-monomers is crucial to prevent phase separation. Introducing functional groups like ethers (–O–), sulfones (–SO_2–), or nitriles (–C≡N) into the polymer backbone can enhance Li-ion coordination and mobility. These groups can also disrupt the polymer's crystalline structure, promoting the amorphous phase and behavior of different organic functional groups, $-CH_3$, $-NH_2$, $-CN$, and $-OH$, in a PEO-based base electrolyte

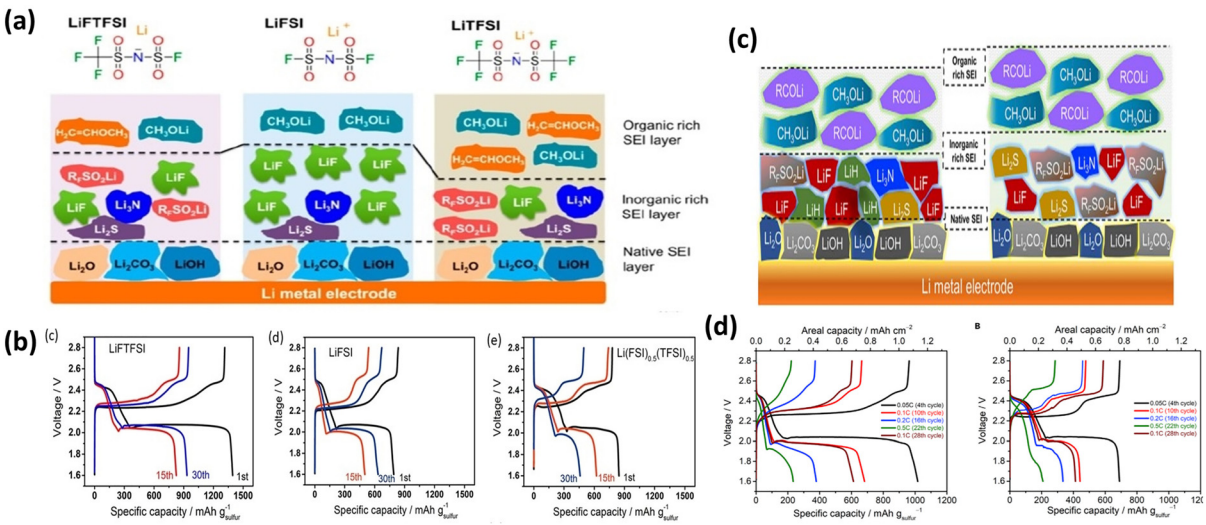

Fig. 10 Interaction of PEO with Li salts with different anions: (a) PEO–LiFTSI, PEO–LiFSI and PEO–LiTFSI; (b) charge–discharge plots of salts in (a); (c) SEI layer formed on Li electrode with LiDFTFSI and LiTFSI salt; (d) charge–discharge plots of salts in (c). These figures have been reproduced from ref. 52 with permission from American Chemical Society copyright 2018 and from ref. 53 with permission Elsevier copyright 2019.

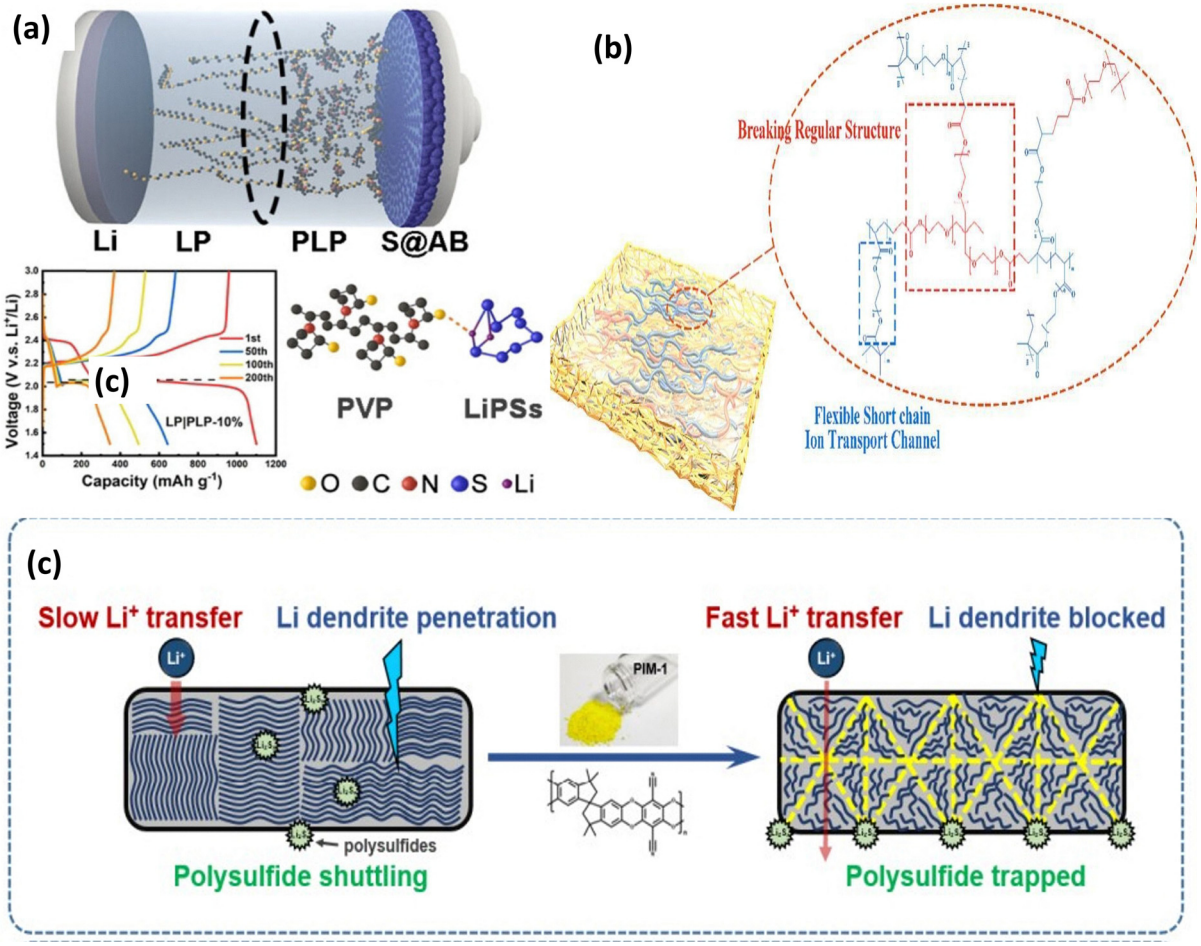

Fig. 11 (a) Scheme of PVP–PEO PE and the charge–discharge plot. This figure is reproduced from ref. 52 with permission from John Wiley and Sons copyright 2022. (b) Synthesis process of UV-cured PPE electrolytes reproduced from ref. 59 with permission from Elsevier copyright 2023. (c) Schematic illustration of PIM reproduced from ref. 57 with permission from John Wiley and Sons copyright 2021.

through molecular dynamics simulations and experimental evidence. In the absence of PEO, calculations suggest a stronger binding order of –CN > –OH > $–NH_2$ > $–CH_3$. Here, the –CN group appears to bind spontaneously with lithium ions due to its high binding free energy (-53.1 kJ mol^{-1}) compared to ether oxygen (-22.8 kJ mol^{-1}). However, when incorporated into the PEO matrix, the binding trend changes. However, the chelating effect of PEO weakens the overall binding strength of functional groups with lithium ions. Additionally, the –CN group cannot form hydrogen bonds with PEO's ether oxygen atoms while coordinating with lithium ions, further reducing its binding favourability. This highlights the importance of considering the complete PEO model when studying Li^+ interactions in PEO-based electrolytes for obtaining accurate results. The trend in lithium ion binding strength follows the order: $–NH_2$ > –OH > –CN > $–CH_3$.[56] Anions exhibit the opposite trend: $–NH_2$ > –CN > –OH > $–CH_3$. These differences in binding interactions influence the room-temperature conductivity and transference numbers of –PEO based SPEs.

PEO/LiTFSI (lithium bis(trifluoromethanesulfonyl)imide) struggled to reach the theoretical capacity of sulfur in the initial cycles and experienced a significantly rapid decline in capacity. However, PEO/LiFSI (lithium bis(fluorosulfonyl)-imide) (Fig. 10a) forms a stable SEI on the Li-anode causing a higher life of batteries.[52] Michele Armand's group has sought to identify a series of lithium salts applicable to LSBs. The PEO/LiDFTFSI combination exhibited a different behaviour. While the $–CF_2H$ groups in LiDFTFSI improved lithium-ion conductivity by reducing anion mobility, they also reacted with PEO (Fig. 10b). Additionally, these groups contributed to a robust SEI on the lithium surface, mitigating the shuttle effect. Consequently, LiDFTFSI-based cells exhibited remarkable cyclability, exceeding 1300 cycles (3000 hours) with near-100% Coulombic efficiencies at 0.1C discharge/charge rates.[53]

Apart from salt modification, copolymers also played a major role in Li–S battery performance. The incorporation of a polymeric layer[57,58] (such as PVDF, PIM, PVP *etc.*) into PEO-based SPEs represents a promising strategy for developing high-performance and long-lasting solid-state Li–S batteries. Fang *et al.*[44] explored the use of a PVDF coating layer, demonstrating its potential in suppressing the formation of soluble lithium polysulfides and promoting a more favourable reaction

mechanism for sulfur by forming a better interfacial contact in the PEO-based SPEs. The PVDF layer is believed to influence the reaction pathway by facilitating a single-step "solid–solid" conversion instead of a multistep "solid–liquid–solid" process typically observed in solid-state lithium–sulfur batteries (Fig. 11a). The presence of only one voltage plateau in the *ex situ* XPS data suggests the direct conversion of short-chain Li_2S_2 to Li_2S during discharge. Additionally, high-resolution cathode mapping reveals an increase in LiS_2^- species after discharge to 1.85 V, with no detectable LiS_4^- signals. This reinforces the notion that elemental sulfur directly converts to solid Li_2S_2/Li_2S, bypassing the formation of long-chain polysulfides during discharge. This effect is likely due to the strong adsorption capability of PEO towards these longer-chain polysulfides. Ao and his team designed a bi-layer composite incorporating a poly(vinylpyrrolidone) (PVP)/PEO layer on the cathode and a PEO/LiTFSI layer on the anode.[19] The PVP layer, with its strong affinity for polysulfides due to amide groups, effectively suppressed polysulfide shuttling (Fig. 11a) with an initial capacity of 1100 mAh g^{-1} and sustained 347 mAh g^{-1} after the 200th cycle at 60 °C.[19] A weight ratio of 3 : 1 for PEO and polyethylene glycol dimethacrylate (PEGDMA) in a PPE polymer electrolyte yielded the best balance of electrochemical performance and the mechanical properties (Fig. 11b). This optimized PPE-1/3 electrolyte enabled Li symmetric cells to cycle stably for over 1600 hours with 929 mAh g^{-1}.[59] Additionally, Li|PPE-1/3|S cells delivered a first-cycle capacity exceeding 900 mAh g^{-1} at 0.2C and maintained a good average Coulombic efficiency (around 95%) after 200 cycles. This promising performance extends to high-capacity Li–S pouch cells.[59] Fig. 11c shows PIM-1 effectively captures lithium polysulfide molecules within a battery and mitigates the detrimental 'shuttle effect' because the electrophilic (electron-attracting) groups in PIM-1, specifically 1,4-dicyanooxanthrene units, bind strongly to the polysulfides. By incorporating PIM-1 into a polyethylene oxide (PEO) composite electrolyte, researchers achieved significant improvements in a lithium–sulfur battery's performance.[57]

2.1.3. Incorporation of plasticizers. PEO–PVP plasticizers act as molecular lubricants, disrupting the polymer's crystalline domains and increasing chain mobility. This translates to superior ionic conductivity but inferior mechanical and structural stability.[60,61] These small organic additives disrupt PEO's crystallinity, enhancing chain mobility and Li-ion transport channels.[60] Highly volatile plasticizers can leach out of the SPE over time, compromising its long-term stability and potentially leading to reduced ionic conductivity. The plasticizer molecules are dispersed throughout the polymer matrix, but they do not form a network. The amount of plasticizer added plays a crucial role in determining whether a material is classified as an SPE or a GPE. A higher concentration of plasticizer can lead to a more continuous liquid phase, pushing the material towards the GPE category. A composite of the PEO_{18}–LiTFSI complex with an ionic liquid consisting of tetraethylene glycol dimethyl ether (TEGDME) shows σ of 6.8×10^{-5} S cm^{-1} (25 °C). Feuillade's group has pioneered the use of an organic plasticizer into a polymer–salt binary system in 1975 for developing quasi-solid-state GPEs.[62] Skaarup and his team incorporated Li_3N, a fast ionic conductor particle as a filler, into the PEO–$LiCF_3SO_3$ matrix.[63] This strategic modification resulted in much higher conductivity of ions surpassing those

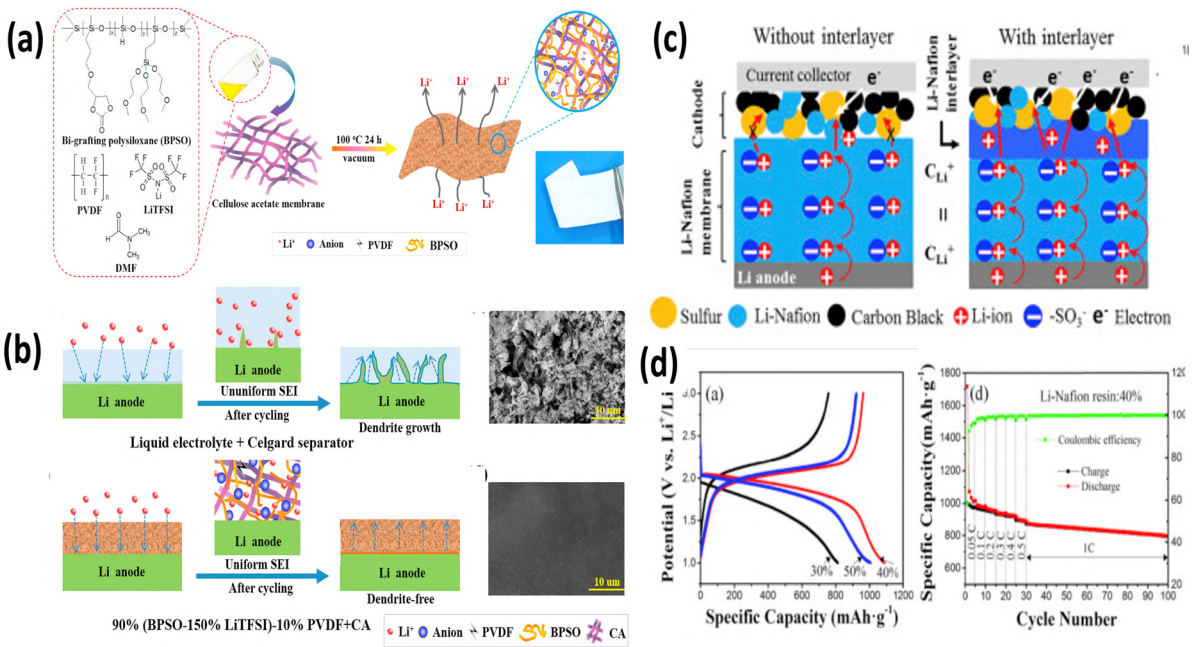

Fig. 12 (a) and (b) Schematic of synthesis and (b) polysulfide shuttling mitigation using a BPSO-polymer electrolyte. The figures are reproduced from ref. 64 with permission from Elsevier copyright 2018, (c) scheme of (d) Li–S battery performance of the Li-Nafion electrolyte. The figures are reproduced from ref. 64 with permission from Elsevier copyright 2018.

of unmodified PEO-based polymer electrolytes. To enhance safety, Cui and his team developed a fire-resistant SPE with PI/DBDPE and PEO/LiTFSI with stable cycling of 300 hours in a Li/PE/Li configuration. Jeedi *et al.* showed that the incorporation of plasticizers into PEO + PVDF/$LiClO_4$ SPEs, *e.g.*, 50 wt% polycarbonate (PC), 4 wt% succinonitrile and 30 wt% dimethyl carbonate, results in conductivities of 2.68×10^{-6} S cm^{-1}, 2.8×10^{-5} S cm^{-1} and 2.53×10^{-6} S cm^{-1}, respectively.[60] Judez *et al.* developed a SPE with lithium bis(fluorosulfonyl)imide ($Li[N(SO_2F)_2]$ + LiFSI/PEO), which exhibited a retarded shuttle effect and high efficiency.

2.1.4. SPEs beyond PEO polymers. Beyond PEO-based electrolytes, PVDF (polyvinylidene fluoride) offers promise for flexible batteries due to its excellent flexibility and processability. Studies have demonstrated the development of SPEs using PVDF as a base material, achieving both high ionic conductivity and strong mechanical properties, leading to improved performance in lithium-sulfur batteries.[64]

Fig. 12(a and b) shows a bi-grafted polysiloxane copolymer with LiTFSI and PVDF. BPSO-150%-LiTFSI-10% PVDF with σ of 7.8×10^{-4} S cm^{-1} at RT, further modified with cellulose acetate, achieving a BPSO-150%-LiTFSI-10%-PVDF + CA polymer electrolyte, shows 91.6% capacity retention after 10 cycles.[64] Other than PVDF, Nafion is also a potential choice for SPEs. Li-Nafion membranes, known for their lightweight and bendable nature, are another attractive option. Their inherent electrical conductivity and ability to block electrons make them suitable for use as both solid electrolytes and

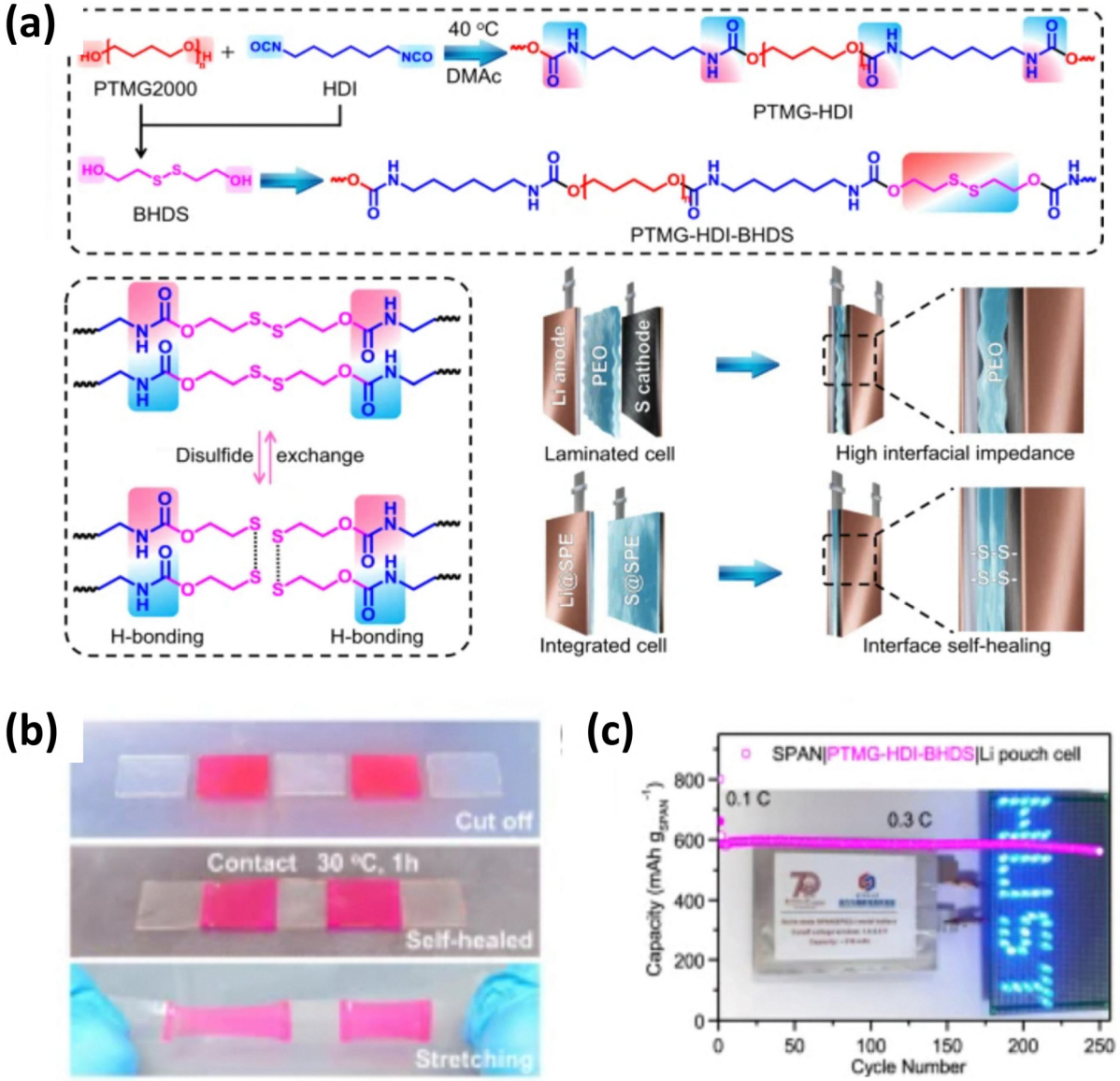

Fig. 13 (a) Schematic depiction of the self-healing mechanism, (b) experimental process of the self-healing mechanism of polymer and (c) demonstration of a LED powered using a pouch cell with a self-healing polymer. The figures are reproduced from ref. 64 with permission from Springer Nature copyright 2024.

Table 1 Li–S battery performance with SPEs

Polymer electrolytes	Cathodes	Ionic conductivity (S cm^{-1}) (temperature)	Li–S battery performance (mAh g^{-1}), retention (%)	Ref.
BPSO-150%-LiTFSI-10% PVDF + CA	MCNT@S	4.0×10^{-4} (25 °C)	987.6 (1st), 91.6% (10th)	64
PIN/SN–LiTFSI	PAN/S	1.15×10^{-4} (RT) 6.55×10^{-3} (80 °C)	500 (1st), 95.2% (50th)	40
PEO–PIM–LiTFSI	S/C	—	1189 (1st), 75.7% (100th)	57
PEO/PVP	S/C	6×10^{-4} (90 °C)	1110 (1st), 31.26% (200th)	19
PEO–PAN–LiTFSI	S/BP-2000(go)	1.63×10^{-5} (below RT)	1110 (1st), 46% (100th)	68
PEO–LiITSI	S@AB	2.58×10^{-5} (30 °C) 1.13×10^{-4} (60 °C)	910 (1st), 12.6% (200th)	59
PPE-1/3 SPE	S@AB	5×10^{-5} (30 °C) 3.2×10^{-4} (60 °C)	1215 (1st), 83.8% (10th) Pouch cells 36.8% (200th), coin cell	59
PEO–LiFSI	SPAN	1.2×10^{-5} (30 °C)	470 (1st), 32% (400th)	67
PTMS–HDI–BHPS–LiFSI	SPAN	6.5×10^{-5} (30 °C)	874 (1st), 93% (700th)	67

separators in LSBs.[65] Researchers have explored the use of PC-Li-Nafion membranes (achieved by swelling Li-Nafion with propylene carbonate) that function as a combined electrolyte and separator (Fig. 12c). This unique structure not only promotes ionic conductivity but also enhances interfacial contact within the battery, ultimately leading to improved specific capacity (Fig. 12(c and d)).[65]

Recently, a lot of polymer electrolyte research studies have also been carried out to develop smart batteries. One of the major areas of smart batteries is self-healing polymer based batteries.[66] Pei and coworkers have developed a best described all-solid-state self-healing polymer electrolyte (PTMS–HDI–BHPS–LiFSI)/poly(ether-urethane) shown in Fig. 13(a and b). The polymer contains various ether-oxygen carbonyl functionalities, and the disruption of these functionalities facilitates improved lithium ion migration, allowing for self-repair of the bond between the electrodes and electrolytes. Ultrasound imaging revealed enhanced contact between these components compared to conventional layers. This better contact helped the sulfurized polyacrylonitrile (SPAN) cathode to last longer (93% after 700 cycles) and work faster (560 mAh g^{-1}). With a sulfur/carbon black (S@CB) cathode, the battery lasted over 350 cycles with 812 mAh g^{-1}. Fig. 13c shows an LED powered by a pouch cell using this polymer electrolyte and SPAN cathode.[67] Electrochemical performances of some reported SPEs for Li–Sulfur batteries are presented in Table 1.

2.2. Gel polymer electrolytes (GPEs)

Though SPEs deliver high safety advantages in the absence of any liquid components, they have limitations like low interfacial stability and low ionic conductivity. Hence, GPEs are introduced to bridge the gap between SPEs and liquid electrolytes. They possess good mechanical strength due to a solid polymer matrix and high ionic conductivity of a minimal liquid component used as a plasticizer. Liquid electrolytes in GPEs help in improving both polymer chain mobility and ionic conductivity. GPEs offer better compatibility with electrodes compared to conventional SPEs, potentially mitigating interfacial issues like lithium dendrite growth and polysulfide shuttling. A good GPE should allow volumetric changes during charge discharge cycles. Fig. 14 shows the essential components of a GPE. Most of the GPE research focuses on tailoring the solid polymer host, liquid plasticizer, and fillers to achieve a balance between mechanical strength, ionic conductivity, and interfacial compatibility.

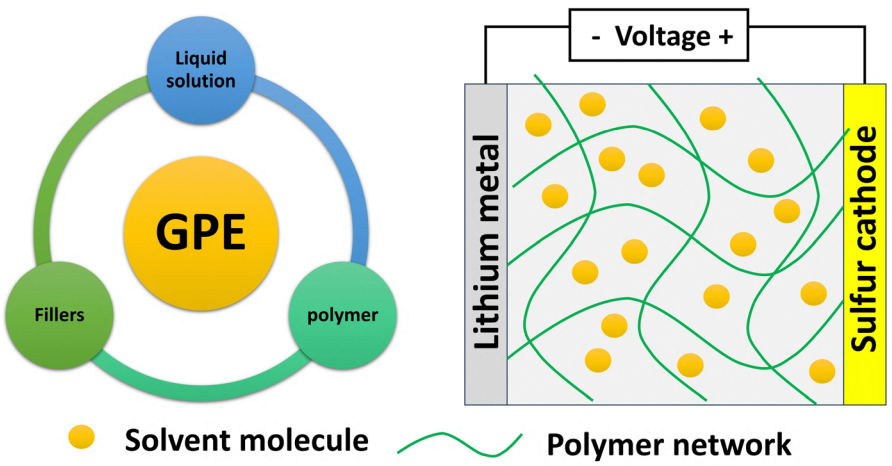

Fig. 14 Schematic diagram of a GPE.

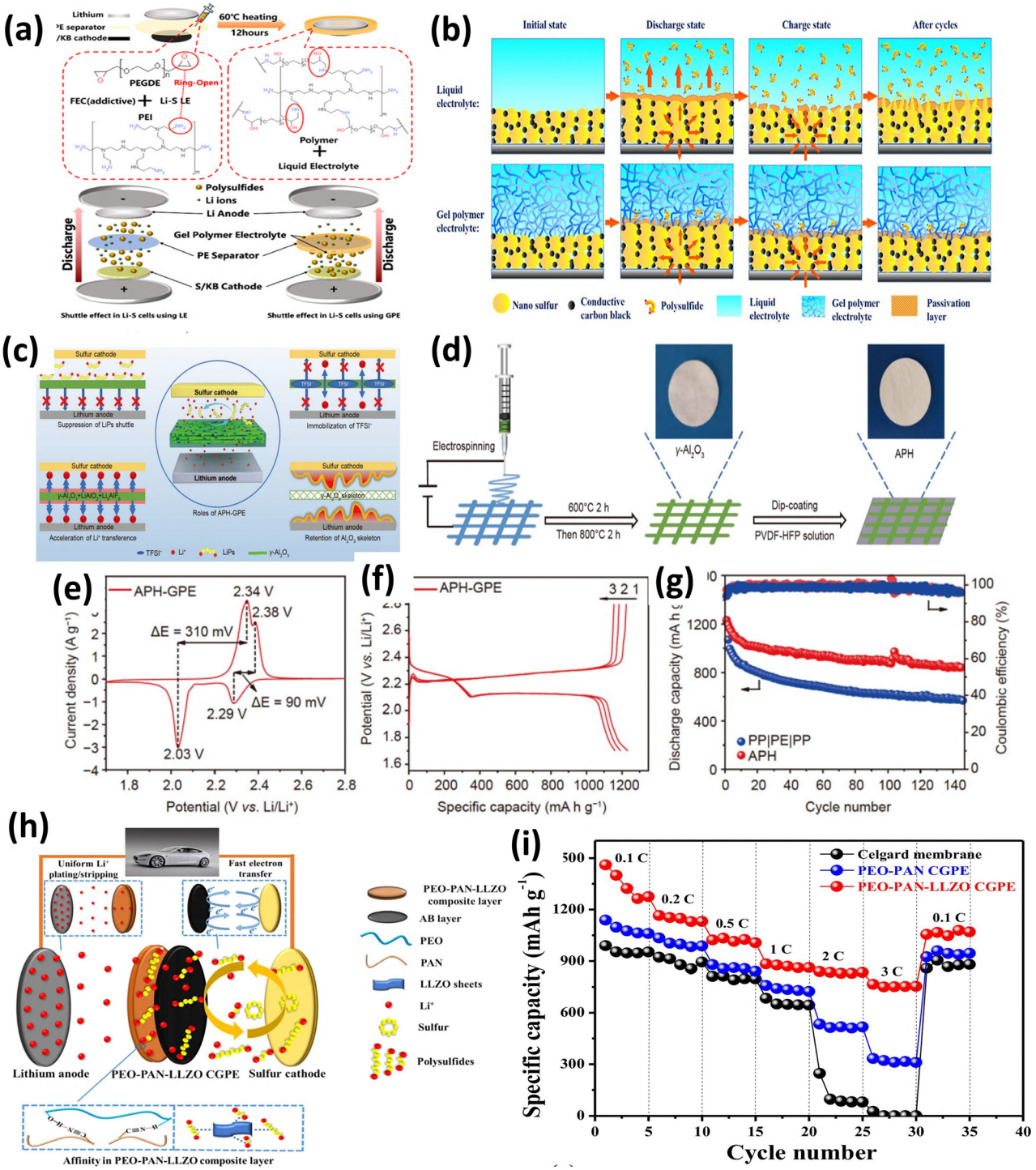

Fig. 15 (a) Cross-linked GPE schematic representation of the shuttling mechanism. The figure is reproduced from ref. 70 with permission from American Chemical Society copyright 2021 and (b) interactions between the cathode, liquid and polymer electrolytes. The figure is reproduced from ref. 70 with permission from American Chemical Society copyright 2021. (c)–(g) Al_2O_3/PVDF-HFP gel polymer electrolyte for Li–S batteries. The figure is reproduced from ref. 70 with permission from Elsevier copyright 2016. (h) and (i) Schematic illustration and rate capability studies of the PEO–PAN–LLZO composite. The figure is reproduced from ref. 70 with permission from Elsevier copyright 2021.

Fig. 15a shows a cross-linked GPE incorporating fluoroethylene carbonate (FEC) to form a solid electrolyte interface (SEI) film. Notably, this GPE is achieved through a simple synthesis process without the need for initiators. The resulting GPE with the FEC additive (GPE@FEC) exhibits an excellent ionic conductivity (0.830×10^{-3} S cm^{-1} at 25 °C and 1.577×10^{-3} S cm^{-1} at 85 °C) and a remarkably high transference number ($t_{Li^+} = 0.674$). Furthermore, GPE@FEC demonstrates a strong ability to anchor

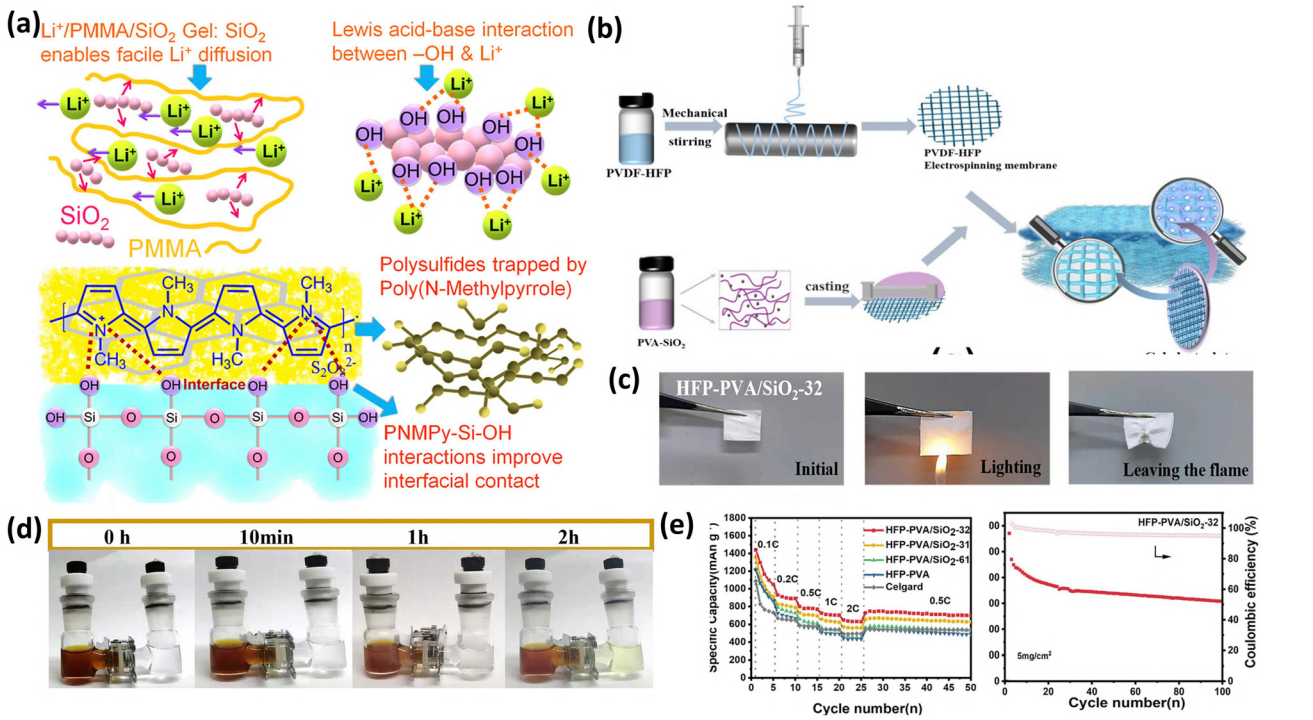

Fig. 16 (a) Poly(*N*-methyl pyrrole) (PNMPy)–SiO_2 mechanism for shuttling inhibition. This figure is reproduced from ref. 74 with permission from American Chemical Society copyright 2018.[75] (b)–(e) Synthesis illustration and (c) LSB studies for the PVA–SiO_2 based GPE. This figure is reproduced from ref. 74 with permission from American Chemical Society copyright 2018.[76]

polysulfides. The exceptional ionic conductivity of this GPE translates to 940 mAh g^{-1} at 0.2C and outstanding cycling performance lasting for 180 cycles at 0.5C.[69] The GPE combines a conductive PVDF-HFP polymer matrix with a high transference number with an electrospun γ-Al_2O_3 nanofiber framework as shown in Fig. 15(c–g). γ-Al_2O_3 facilitates structural stability, and the Lewis acid–base interaction of the γ-Al_2O_3 nanofiber-polymer network suppresses polysulfide shuttling (841.5 mAh g^{-1} capacity at the end of 150 cycles at 0.1C with low decay) and promotes Li salt dissociation (1000 h stable operation at 0.5 mA cm^{-2}). Fig. 16h shows a PEO–PAN–LLZO composite GPE membrane, which possesses outstanding mechanical and interfacial properties. It efficiently absorbs the electrolyte, inhibits the "shuttle effect", and safeguards the lithium anode (Fig. 16i), leading to enhanced rate capability. The CGPE based Li–S battery displays 1459/942 mAh g^{-1} at 0.1/1C and 555 mAh g^{-1} at 1C after the 500th cycle.[70] Liu *et al.* introduced a pentaerythritol tetra acrylate (PETEA)-based GPE that addresses the polysulfide shuttling problem.[71] The robust PETEA matrix and its flexible passivation layer effectively suppresses polysulfide movement (dissolution). This innovative GPE exhibits an exceptionally high σ of 1.13 × 10^{-2} S cm^{-1}, a gravimetric capacity of 601.2 mAh g^{-1} at 1C and 81.9% (@0.5C) capacity retention after the 400th cycle due to the packed Li_3N layer formed at the electrode–electrolyte interface. Peng-Qin Wang *et al.*[36] reported a poly (1,3-dioxolane) (PDOL)-g-C_3N_4 thick film, with σ of 3.7 × 10^{-4} S cm^{-1}, which was stable up to 5.0 V and helped in dendrite suppression. A capacity of 1150/550 mAh g^{-1} was achieved at 0.1/1C with 83% retention after the 100th cycle.[72] Chiu and coworkers reported a polymethyl methacrylate (PMMA)-based GPE for lithium–sulfur cells with a high-loading cathode (S loading: 8–10 mg cm^{-2}), showing 7.1 mAh cm^{-2} and 15 mW h cm^{-2}.[73]

Fig. 16a shows the uniform coating of a conducting Poly(*N*-methyl pyrrole) (PNMPy) polymer with an σ about 1 mS cm^{-1}. Li/PMMA/SiO_2 GPE with a Li–S@RGOPNMPy cathode shows 100% CE after the 500th cycle.[75] Hui and coworkers have reported an asymmetric and structurally stable SiO_2@PVA/PVDF-HFP, Fig. 16(b–e). These asymmetrically coated PVDF-HFP membranes exhibited excellent wettability, which is crucial for effective gelling with good ionic conductivity, surpassing that of traditional Celgard separators. With 90% sulfur cathode, this gel electrolyte exhibited 1439 mAh g^{-1} at 0.1C with high cycling.[76] Table 2 shows the GPE performances for Li–S batteries.

2.3. Composite polymer electrolytes

CPEs are designed to solve the limitations pertinent to both SPEs and GPEs. Unlike SPEs, CPEs incorporate inorganic fillers which improve ionic conductivity, and suitable fillers help improve the mechanical strength.

2.3.1. Components of CPEs. Three key components contribute to the functionality of CPEs as described in Fig. 17:

2.3.1.1. Polymer matrices. These flexible backbones, often based on materials like PEO, PVDF, or PPC, provide structural

Table 2 GPE performances for Li–S batteries

Polymer	Liquid electrolytes[a]	σ (10^{-4} S cm^{-1})	Li–S performance (initial (mAh g^{-1}, retention (%))	Ref.
PAN–PEO–LATP	Std. + 1 wt% $LiNO_3$	8.61	1200 (1st), 80% (300th)	77
MOF–PVDF GPE	Std. + 1 wt% $LiNO_3$	—	1381 (1st), 72% (200th)	78
PVdF/PEO–ZrO_2	Std.	0.525	1059, 847.2 (500th)	79
PVdF	Std. + 0.4 M $LiNO_3$	3	1675, 1000 (100th)	80
PVdF-HFP–SiO_2	1 M LiTFSI/PMImTFSI	1.1	1029, 885 (30th)	81,82
PEO	Std. + 2 wt% $LiNO_3$	1.76	1182, 648 (100th)	82
PVdF/organo-polysulfides	0.6 M LiTFSI in DEM/DOL + 0.4 M $LiNO_3$	0.708	843, 484 (300th)	83
PPC SiO_2	Std. + 1 wt% $LiNO_3$	0.164	1672, 1422.1 (500th)	84
PAA	0.25 mol kg^{-1} LiTFSI in DME/DOL + 0.25 mol kg^{-1} $LiNO_3$	—	1012, 800 (40th)	85
PMMA/PMPTMS/PVdF-HFP–SiO_2	1 M $LiPF_6$ in EC/DEC	3.009	895, 845 (100th)	75
PMMA–SiO_2	Std. + 0.2 M $LiNO_3$	1.1	1197, 476 (500th)	86
PVdF-HFP–Al_2O_3	Std. + 0.1 M $LiNO_3$	3.0	1150, 71 (100th)	87
PVdF-HFP–LATP	Std. + 1 wt% $LiNO_3$	0.331	918, 458.9 (40th)	88
PEO–LAGP	1 M LiTFSI in TEGDME	1.15	725, 700 (300th)	89
PEGDA–LLZTO	Std. + 1 wt% $LiNO_3$	1.34	1201, 656 (200th)	90
PVDF-HFP–Al_2O_3	Std. + 0.2 M $LiNO_3$	1.35	841.5 (100th)	91
PMMA–SiO_2	Std. + 1 wt% $LiNO_3$	0.385	200 (500th)	75
PVA–SiO_2	Std. + 1 wt% $LiNO_3$	1.28	1439, 71% 500th, (low loading)	84
PVA–SiO_2	Std. + 1 wt% $LiNO_3$	—	54% (100th), high loading	84

[a] std: 1M LiTFSI in DOL/DME.

integrity and safety. Their development has been ongoing from 1973 regarding Li^+-ion mobility in PEO.[92,93]

2.3.1.2. Lithium salts. Lithium salts (*e.g.* LiFSI, LiTFSI *etc.*) dissolved in a polymer matrix provide mobile lithium ions for battery operation. This choice of salts ensures the conductivity and stability of CPEs.

2.3.1.3. Inorganic fillers. These ceramic or inorganic additives (*e.g.* SiO_2, Al_2O_3, LLZO *etc.*) can control the properties of CPEs by tuning the mechanical properties and ionic conductivity, which helps in battery performance.

The first demonstration of a polymer–ceramic composite electrolyte came in 1982, achieved by incorporating an Al_2O_3 in the PEO matrix.[31] This resulted in improvements in both the mechanical strength and ionic conductivity. In 1992, a study systematically investigated the effects of the wt% and particle size of a functional filler, $LiAlO_2$, on the performance of CPEs.[94] Later, PEO with mesoporous lithium aluminate was explored, which has been proved to show high ionic conductivity on filler introduction.[95] Similarly, studies have shown that introducing LLTO, LLZO, and LLAZO fillers contributes to both mechanical and ionic conductivity improvements.[93,96,97] Fig. 18 shows Li-ion conductivity of a few inactive and active fillers researched over the years.

2.3.2. Li^+ conduction mechanism in CPEs. Optimizing the design of composite electrolytes for lithium batteries hinges on understanding Li^+ ion transport pathways. In these systems, Li^+

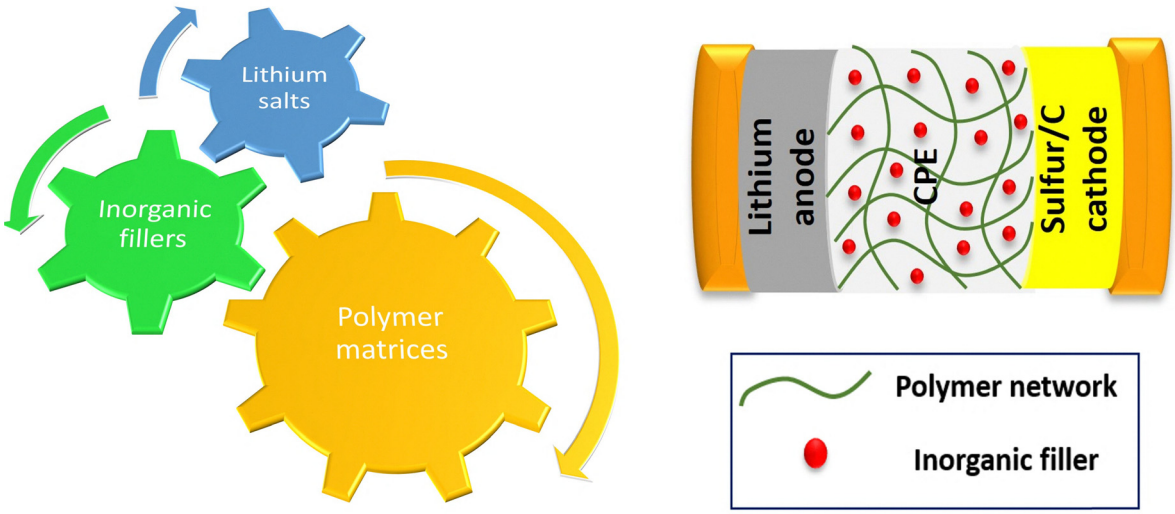

Fig. 17 Schematic diagram of a composite polymer electrolyte.

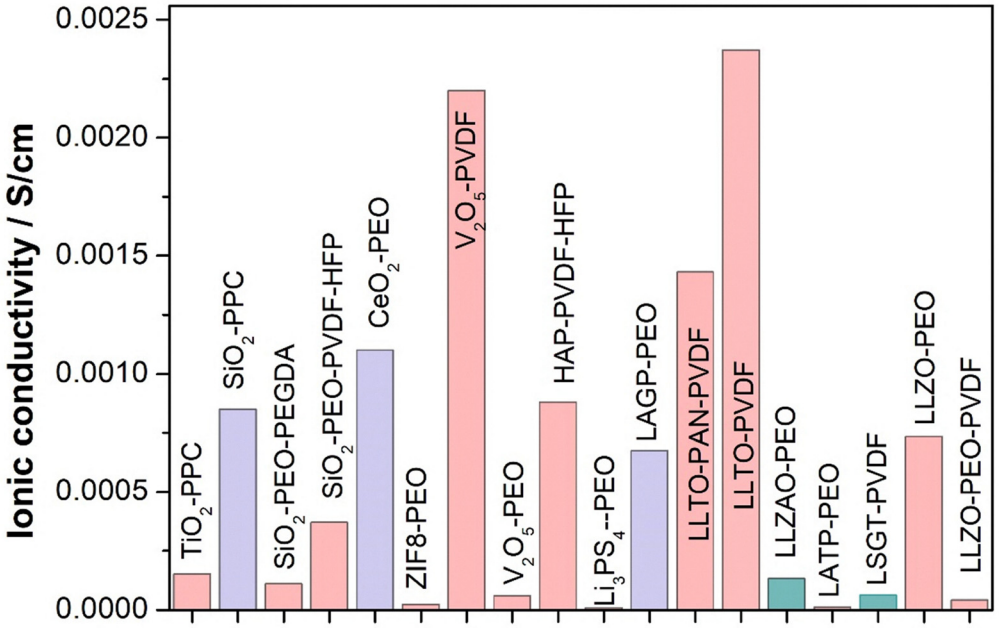

Fig. 18 Ionic conductivity performance of different CPEs based on recent works (pink: room temp, purple: 60 °C, green: 20 °C).

ions can migrate through three main regions: the polymer matrix itself, the dispersed ceramic fillers, and the critical interface between them. Zhang *et al.* (Fig. 19a) suggest three main pathways for ion migration: the polymer phase, the ceramic phase (fillers), and the interface between them In CSEs with a low ceramic content, the isolated ceramic particles do not create a continuous path for ions, neither within themselves nor at the interface with the polymer.[98] Consequently,

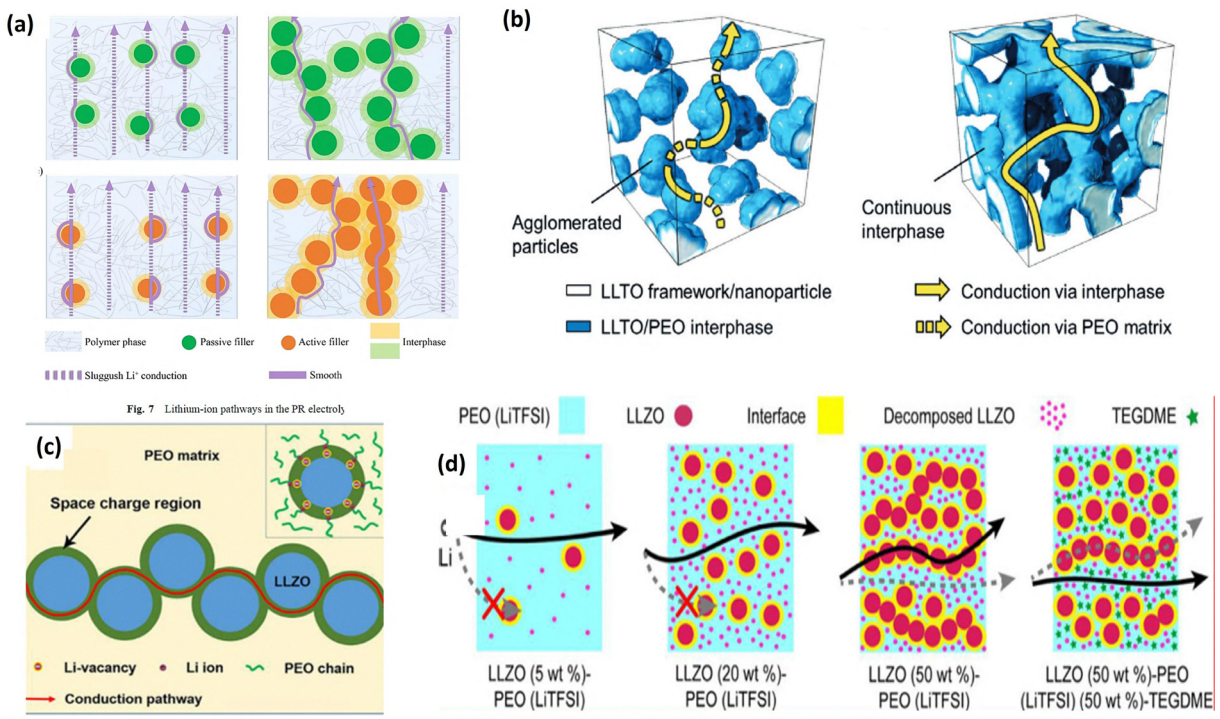

Fig. 19 Ion conduction mechanism in a CPE. (a) Ion conduction in active and passive fillers. This figure is reproduced from ref. 101 with permission from American Chemical Society copyright 2018. (b) Ion conduction in the LLZO nanofiber framework. This figure is reproduced from ref. 102 with permission from American Chemical Society copyright 2018. (c) Ion conduction through the space charge region at the interface between a ceramic filler (Ga-LLZTO) and the polymer matrix (PEO).[93] (d) NMR studies and ion conduction in LLZO–PEO–TEGDME composites. This figure is reproduced from ref. 74 with permission from American Chemical Society copyright 2018.

ion movement relies primarily on the polymer phase. Here, both passive and active fillers can improve conductivity by reducing polymer crystallinity. The actual conductivity of the bulky ceramic itself contributes minimally to the overall performance of the composite electrolyte. With the increase in the ceramic content, a continuous network of ceramic particles forms, creating a well-connected interface region. In these CPEs, fillers (active or passive) that promote continuous ion conduction through this abundant interface can significantly enhance overall conductivity. However, active fillers can provide additional migration pathways, further increasing conductivity diversity.[99] Not only the composition but also the morphology of these fillers plays a major role in governing the ionic path of conduction. Traditional nanofillers like LLTO particles can initially improve conductivity following a percolation model (Fig. 19b). However, as their concentration increases, they tend to clump together, reducing the crucial interface area and disrupting ion transport pathways. Conversely, 3D LLTO frameworks, fabricated using methods like sol–gel, offer a significant advantage. Their pre-designed, interconnected structure prevents particle agglomeration and maintains a continuous network for efficient Li-ion movement throughout the electrolyte, even at higher filler loadings.[100,101] Fig. 19c shows that using transmission electron microscopy (TEM), a space charge region was identified at the interface between a ceramic filler (Ga-LLZTO) and the polymer matrix (PEO). This finding suggests that these interfacial regions may act as efficient Li+ ion transport channels, potentially explaining the observed increase in ionic conductivity.[93] This hypothesis was further supported by Monte Carlo simulations. Through high-resolution solid-state Li NMR and selective isotope labeling, Hu and team identified the LLZO ceramic phase as the primary pathway for lithium ion conduction in a PEO/LLZO/$LiClO_4$ composite with a 50 wt% $Li_7La_3Zr_2O_{12}$. With lower concentration of LLZO, the migration happens through the polymer phase and with higher concentration of LLZO, it happens through the ceramic phase for the PEO/LLZO/LiTFSI system.[74] With introduction of a plasticizer like TEGDME, lithium ions moved preferentially through the PEO–TEGDME matrix.[74] Table 5 shows the Li^+ ion conductivity of a few inactive and passive fillers.

2.3.3. Active and inactive fillers for shuttling inhibition. To improve the mechanical and electrochemical properties of SPEs in lithium–sulfur batteries, researchers incorporated inorganic fillers. These ceramic fillers, (*e.g.* Al_2O_3,[91,103,104] MOF,[105] V_2O_5,[106] SiO_2,[75] ZIF[107]) have been introduced into polymer electrolytes. Fillers like nano Al_2O_3 disrupt the PEO's crystallization process and create more amorphous domains within the material, which are favourable for lithium ion transport, leading to enhanced ionic conductivity.[104] Two dimensional (2D) materials have also been used as fillers for Li–S batteries and proved to be effective for the mitigation of polysulfide shuttling, with good thermal and mechanical stability.[108,109] Boron nitride (BN) fillers for PEO–PVDF play a major role with temperature stability due to its thermally conducting nature. IR images (Fig. 20a) of BN based polymer electrolytes confirm a faster thermal transport in the presence of BN flakes. Upon switching the temperature to 70 °C from RT, the BN–PEO–PVDF electrolyte exhibits a faster rise in ionic conductivity as well, reaching a stable value of approximately 2×10^{-4} S cm^{-1} within 300 seconds. In contrast, pristine one requires over 700 seconds to achieve a lower stabilized value of around 0.6×10^{-4} S cm^{-1}. Cells utilizing the BN–PEO–PVDF electrolyte exhibit high discharge potential compared to the PEO–PVDF electrolyte across various test temperatures[108] and higher capacities (around 1200 mAh g^{-1} initially and 790 mAh g^{-1} after 50 cycles) and maintains good performance at higher discharge rates (750 mAh g^{-1} at 1/5C). This improvement holds true even at lower temperatures (1000 mAh g^{-1} at 55 °C). Liu *et al.* showed incorporating Nb_2CT_x MXene into a PEO-based polymer electrolyte not only boosted lithium ion (Li^+) conductivity but also enhanced polysulfide adsorption, a critical factor for battery stability.[109] Moreover, the sheet size of Nb_2CT_x MXenes helps in Li^+ conductivity and polysulfide absorptivity, pertaining to the percolation effect.[109] Size modulation of Nb_2CT_x-MXenes from the sub-nano to nanometer range resulted in σ of 2.62×10^{-4} S cm^{-1} with improved t_{Li^+} of 0.37 at 60 °C. Furthermore, among them, higher binding energy of long-chain polysulfides (Li_2S_n (n = 4, 6, 8)) of Nb_2CT_x (Fig. 20b) implies better entrapment of polysulfide species, further validated by X-ray photoelectron spectroscopy (XPS) and UV-Vis spectroscopy measurement. ASSLSB exhibits a capacity of 1149 mAh g^{-1} at 0.5C and a cycling stability of 491 mAh g^{-1} after 200 cycles. Li *et al.* proposed a strategy of using ordered MIL-125-NH_2 fillers within a polymer electrolyte (Fig. 20c), and the resulting 3D MPPL CPE achieved better transport ($\sigma = 8.3 \times 10^{-4}$ S cm^{-1} at 60 °C) compared to conventional electrolytes. Raman studies confirmed that the structure enables better adsorption of LPS compared to MPL–CPE for the 3D MPPL CSE, resulting in efficient inhibition of polysulfide shuttling. Pouch-type ASSLSBs using the 3D MPPL CPE demonstrated impressive cycling stability, exceeding 400 cycles at moderate current densities (0.5C) and 60 °C, highlighting the effectiveness of this approach in achieving high-performance ASSLSBs.[105]

2.3.4. Active fillers: boosting conductivity and suppressing degradation. Researchers are exploring lithium-ion conducting active fillers for composite electrolytes instead of only strengthening the electrolyte with passive fillers, for solid state lithium-sulfur batteries. These fillers are not passive bystanders; they actively participate in the battery operation. By conducting lithium ions themselves, active fillers (*e.g.* LLTO,[110] LLZTO[97] *etc.*) significantly enhance the overall conductivity of the electrolyte. This translates to improved battery performance by mitigating a major degradation pathway – polysulfide dissolution. By effectively capturing these polysulfides, they help prevent them from shuttling within the battery and causing declining performance. Judez *et al.* explored LiFSI/PEO/Al_2O_3 and an active LICGC filler to improve the stability of the Li/PE interface (Fig. 21a), however, cells utilizing the LICGC-incorporated composite electrolyte exhibited exceptional performance, showing capacities of 1111 mAh g^{-1}/1.14 mAh cm^{-2}. The Li–S cells with a bilayer electrolyte showed 99% capacity

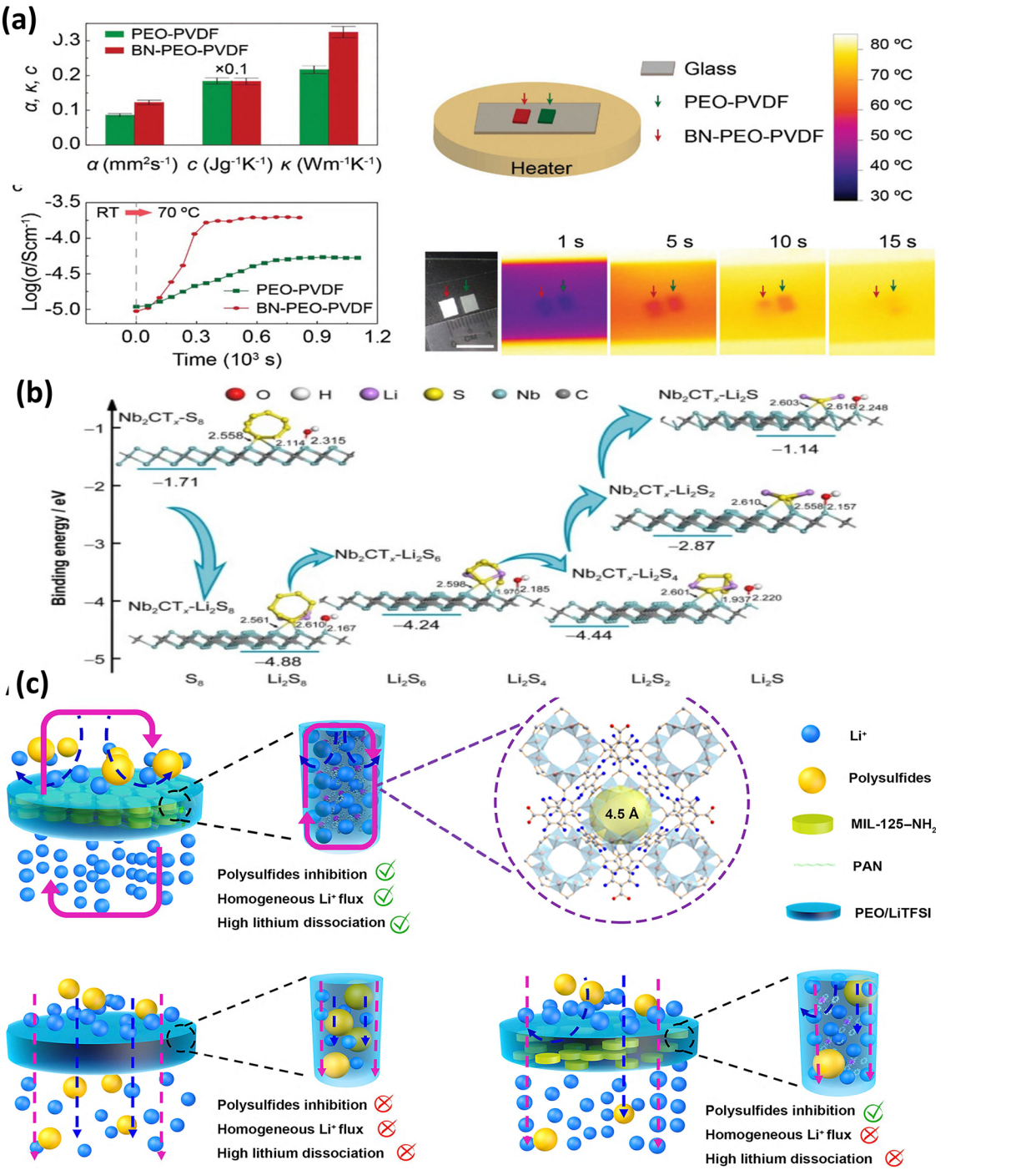

Fig. 20 (a) Ionic and thermal conductivity at different temperatures for different durations for BN–PEO–PVDF polymer electrolytes. This figure is reproduced from ref. 108 with permission from American Chemical Society copyright 2018. (b) Polysulfide binding energy calculations for Mxene-Nb_2CT_x-PEO. This figure is reproduced from ref. 109 with permission from Springer Nature copyright 2023. (c) Schematic illustration of shuttling in MIL-125-NH_2/PEO-LiTFSI electrolytes. This figure is reproduced from ref. 105 with permission from AAAS copyright 2024.

retention after 50 cycles at 70 °C (Fig. 21a). Later, a PEO/LiTFSI/$LiSnP_2S_{12}$ CPE delivered a high capacity of 1016 mAh g^{-1} (0.1C, 60 °C). A novel solid-state lithium-sulfur battery achieved a breakthrough by combining a conductive electrolyte (0.42×10^{-3} S cm^{-1}) with a sulfur-polyacrylonitrile (S/PAN) cathode with its innovative polymer electrolyte design (Fig. 21b). This design delivered 1772 mAh g^{-1} at 0.1C and 719 mAh g^{-1} at 0.5C. The secret lies in the design's ability to promote efficient lithium-ion movement (0.87 Li^+ transference number) and mitigate volume changes within the cathode, leading to superior performance. Other studies explored composite SPEs with LLZO (garnet-type) and ionic liquid-modified nanoparticles,

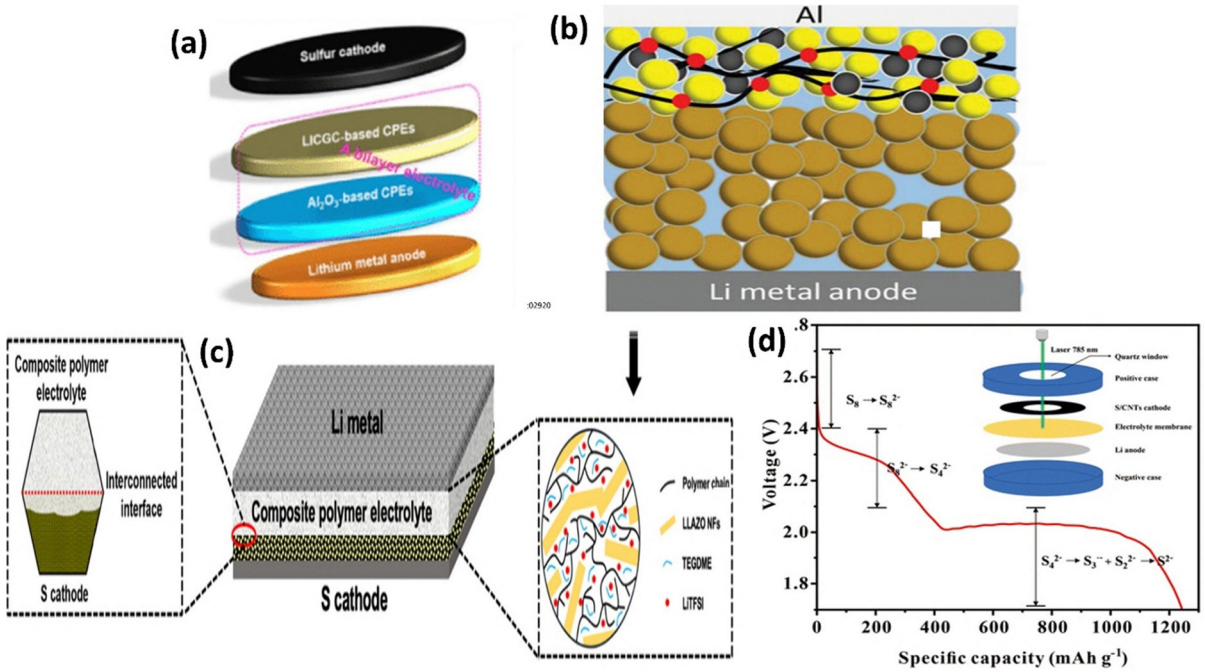

Fig. 21 (a) Battery schematic of 3 vol% Al_2O_3/LICGC-CPEs. This figure is reproduced from ref. 74 with permission from American Chemical Society copyright 2018. (b) Schematic & CD curves of S@LLZO@C|S@C at 37 °C. This figure is reproduced from ref. 74 with permission from American Chemical Society copyright 2018.[111] (c) LLZO based Garnet-CPE. This figure is reproduced from ref. 74 with permission from American Chemical Society copyright 2018.[111] (d) Discharge curve (inset: Raman cell) of S@CNT|LLZTO/HUT|PEO|Li. This figure is reproduced from ref. 97 with permission from American Chemical Society copyright 2018.

showing good conductivity and Li–S batteries with capacities exceeding 900 mAh g^{-1} and maintained for 200 cycles.[105] Garnet-shaped nanofibers (LLAZO NFs) are incorporated which boost σ at RT, 5.71 × 10^{-4} S cm^{-1}, suppress polysulfide diffusion, and enhance mechanical strength.[111] The LLAZO NFs also contribute to a low activation energy (0.268 eV) and a high t_{Li^+} (0.70). As a result, a prototype all-solid-state Li–S battery using this CPE demonstrates exceptional cycling stability over 100 cycles and promising rate performance at room temperature (Fig. 21c). Wang *et al.* have demonstrated LLZTO nanoparticles modified with a zwitterionic layer (LLZTO@-HUT4) (Fig. 21d). The resulting LLZTO@HUT4-15%/PEO electrolyte exhibited a high ionic conductivity (0.73 mS cm^{-1} at 60 °C) and efficient lithium ion transport (transference no = 0.74), leading to a promising initial discharge capacity (1018 mAh g^{-1} at 0.2C) and around 92% capacity retention after 100 cycles in a lithium–sulfur battery test.[97] The zwitterionic layer improved lithium ion movement and strengthened the inorganic nanoparticles/polymer electrolyte interface (Fig. 21d). Table 3 shows the lithium sulfur battery performance with active and inactive filler based composite electrolytes.

2.4. Enhancing mechanical and electrochemical stability with polymer electrolytes

The development of high-performance polymer electrolytes for solid-state batteries hinges on balancing mechanical robustness with exceptional ionic conductivity. A deep dive into the properties of various polymer electrolytes reveals key insights

Table 3 Lithium–sulfur battery performance of active and inactive filler based composite electrolytes

Polymer electrolyte	Cathode	σ (S cm^{-1})	Li–S battery performance (mAh g^{-1}), retention (%)	Ref.
PEO–PVDF–BN	C/S	8.61 × 10^{-4}	1200 (1st), 80% (300th)	108
PEO–LGPS	PAN/S	4.2 × 10^{-4}	1383 (1st), 42.5% (50th)	112
PEO–LLZO NF	C/S	5.71 × 10^{-4}	915 (1st), 56.7% (100th)	111
EO-xLSPSCl-LiTFSI	C/S	3 × 10^{-4}	1675 (1st), 80% (500th cycles)	41
PEO_{18}–LiTFSI–LLZO–SN	PAN/S	1.16 × 10^{-4}	1029 (1st), 81.2% (60th cycles) at 0.2C	113
PEO–LLZTO@HUT4	S/C	0.73 × 10^{-3} (60 °C)	1182 (1st) 92.1% (100th)	97
PEO–Al_2O_3–LiTFSI–PTFE	CNTs/S	—	1415 (1st), 45.2% (120th)	114
Vr/PEO-LCSE	S/C	12.2 × 10^{-4} at 25 °C	1200 (1st), 76.6% (100th)	115
PEO-LGPS	PAN/S	4.2 at RT	1183 (1st), 49.8% (50th)	116
PEO-IL@NPs/ZrO_2	S/C	4.95 × 10^{-4} (50 °C) 2.32 × 10^{-4} at (37 °C)	986 (1st), 80%	117
PEO–LSPS	PAN/S	1.69 (60 °C)	1016 (0.1C, 60 °C)	118
PEO-Nb_2CT_x-MXene	S/C	2.62 × 10^{-4}	1149 (1st), 40% (200th)	109
PEO/$LiBH_4$/SiO_2	S/C	4.09 (70 °C)	967 (70 °C)	119

Table 4 Mechanical strength and ionic conductivity of different polymer electrolytes for solid state Li-batteries[120]

Fiber	Matrix	L μm	Tensile strength (MPa)	Galvanostatic metal stripping/plating cycle test lifespan	Ref.
Polyimide NFs	LLZTO/PVDF/LiTFSI	20	11.5	1000 h (0.1 mA cm^{-2}) at 25 °C	121
Polyimide NFs	PEO/LiTFSI	17.5	13.9	500 h (0.1 mA cm^{-2}) at 25 °C	122
PVDF/TBAC salt NFs	PEO/LiTFSI	60–80	7.8	1000 h (0.3 mA cm^{-2}) at 70 °C	123
β-PVDF-HFP NFs	PEO/LiTFSI	230–300	0.45	>600 h (0.2 mA cm^{-2}) at 60 °C	124
PAN NFs	PEO/LLZTO/SN/LiTFSI	75.7	3.45	500 h (0.1 mA cm^{-2}) at 45 °C	125
PAN NFs	PEO/LiTFSI/PDMS	50	9.64	1200 h (0.3 mA cm^{-2}) at 60 °C	126
Partially cyclized PAN NFs	PEO/LiTFSI	30	2	2000 h (0.25 mA cm^{-2}) at 25 °C	127
PAN NFs grafted with lithiated, branched PEI	PEO/LiTFSI	120	8.9	900 h (0.2 mA cm^{-2}) at 60 °C	128
Polyamide 6 (PA6)	PEO/LiTFSI/SN	85	4.52	400 h (0.1 mA cm^{-2}), 1000 h (0.05 mA cm^{-2}) at 30 °C	129

into their strengths and weaknesses. Table 4 presents a summary of various polymer electrolytes incorporating different fibers and matrices, highlighting their tensile strength and cycling lifespan. The table shows that polyimide nanofibers (NFs) in a poly(ethylene oxide) (PEO)/LiTFSI matrix demonstrate a high tensile strength of 13.9 MPa and a cycle lifespan of 500 hours at 25 °C.[15] In contrast, the same fiber type combined with an LLZTO/PVDF/LiTFSI matrix offers a slightly lower tensile strength of 11.5 MPa but a longer lifespan of 1000 hours under similar conditions, suggesting that the matrix composition is critical for long-term stability [14]. Materials like polyacrylonitrile (PAN) NFs and their derivatives, such as partially cyclized PAN NFs, show impressive performance. Partially cyclized PAN NFs, for instance, exhibit a lifespan of 2000 hours, the longest among the listed materials, despite having a relatively low tensile strength of 2 MPa.[21] This indicates that chemical modifications, like cyclization, can significantly enhance electrochemical stability, which is vital for commercial applications. Conversely, the β-PVDF-HFP NFs show the lowest tensile strength at 0.45 MPa but still manage a respectable lifespan of over 600 hours at 60 °C.[17] The data suggest that while high mechanical strength is desirable, it does not always directly correlate with a longer lifespan, and other factors, such as the operating temperature and current density, play a significant role.

2.5. Solid state Li–S batteries with Li_2S cathode

A particularly appealing configuration involves utilizing Li_2S as the cathode, which, being a prelithiated compound, facilitates the design of ''lithium-metal-free'' Li–Sulfur batteries. This mitigates the safety concerns associated with metallic lithium anodes and allows for the integration of high-capacity alternative anode materials like silicon–carbon (Si/C), tin–carbon (Sn/C), and carbon (C) composites. The synergistic combination of a Li_2S cathode, these advanced anodes, and polymer electrolytes (PEs) offers a robust pathway towards high-performance and safer Li–S systems. Li_2S cathodes offer the distinct advantage of allowing the use of Li-free anodes, simplifying battery assembly and improving safety. Conceptually, they also bypass the initial formation of soluble lithium polysulfides, reducing the infamous shuttle effect.[130–134] However, Li_2S is intrinsically insulating, requiring significant conductive additives, and suffers from a high activation overpotential during the first charge. Moreover, its substantial volume change (~80%) during cycling can disrupt cathode integrity. To complement the Li_2S cathode, high-capacity, Li-free anodes such as Si/C, Sn/C, and C are explored. Silicon (theoretical capacity ~4200 mAh g^{-1}) and tin (theoretical capacity ~994 mAh g^{-1}) offer high energy density but undergo drastic volume changes upon lithiation (~300–400%). Carbon hybridization (Si/C, Sn/C) is crucial to buffer these volumetric expansions, enhance electronic conductivity, and improve structural stability.[135] Carbon (C) anodes, like hard carbon, provide greater volume stability and good cycling performance, albeit with lower specific capacities than Si or Sn. However, the intrinsic ionic and electronic insulating nature of Li_2S poses challenges to its electrochemical activation in solid-state systems. Achieving high Li_2S utilization in ASSLSBs necessitates excellent interfacial contact between the active material, the solid electrolyte, and conductive carbon. Furthermore, the kinetics of Li_2S oxidation, particularly the initial activation, can be sluggish, requiring higher charge overpotentials compared to subsequent cycles.

Recent advancements demonstrate that concepts developed for liquid electrolytes, such as nanoscale encapsulation and electrocatalysis, are translatable to SPE-based ASSLSBs. For instance, Li_2S@TiS_2 core–shell structures facilitate efficient LiPS trapping within the particles, confirmed by *in situ* characterization. Crucially, the TiS_2 layer actively catalyses the oxidation of Li_2S, significantly lowering reaction energy barriers (*e.g.*, from 1.73 eV to 0.57 eV for Li_2S to Li_2S_2 conversion). This catalytic effect, corroborated by density functional theory (DFT) calculations, enables higher specific capacities, reaching up to 910 mAh g^{-1} Li_2S, and improved cycle life.[136] The integration of such optimized Li_2S cathodes with SPEs and Li metal anodes has yielded an impressive cell-level specific energy of 427 Wh kg^{-1} surpassing those of most reported ASSLSBs. This underscores the potential of interface engineering and catalytic designs to overcome the inherent limitations of Li_2S in the solid state, paving the way for truly robust and high-performance ASSLS batteries. Bruno Scrosati and group demonstrated a lithium-metal-free tin–sulfur battery employing a Sn/C anode, a Li_2S/C cathode, and a polyethylene oxide/lithium trifluoromethanesulfonate (PEO/$LiCF_3$ SO_3) polymer matrix

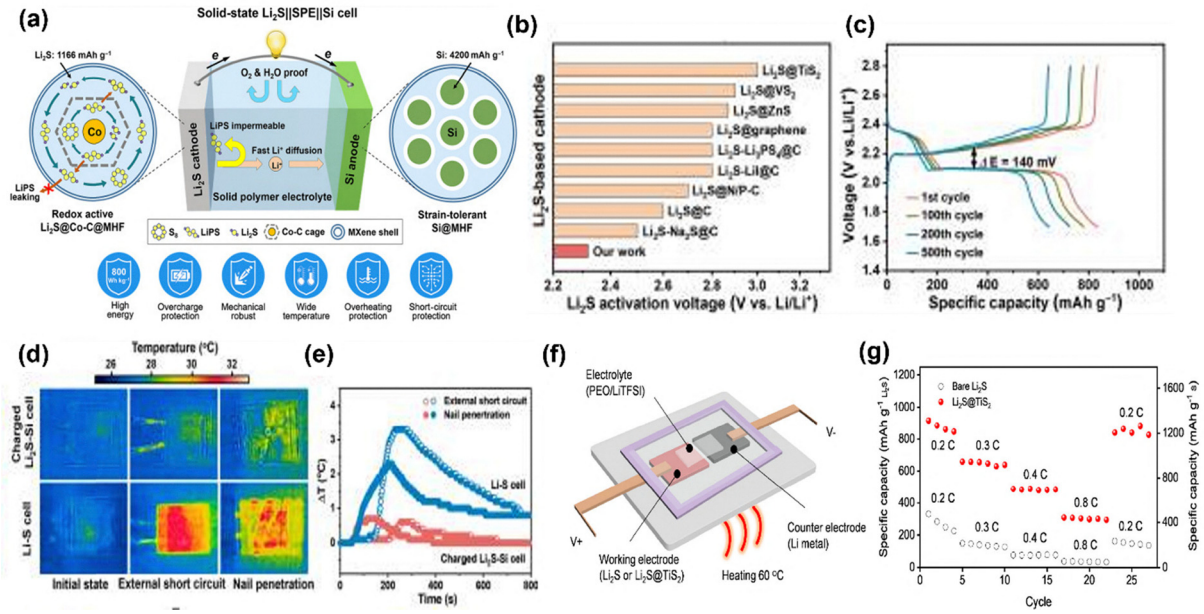

Fig. 22 (a) Schematic diagram of Si/C anode|Li_2S cathode, (b) comparison of different Li_2S based cathode activation voltage, (c) charge discharge curve at different cycles, (d) external short circuit and nail penetration, and (e) temperature simulation for the Si/C anode. These figures are reproduced from ref. 137 with permission from AAAS copyright 2022. (f) Schematic of TiS_2 anode|Li_2S cathode (g) rate capability studies of TiS_2 anode|Li_2S cathode. This figure is reproduced from ref. 138 with permission from American Chemical Society copyright 2020.

based gel polymer electrolyte (CGPE).[137] This setup achieved an energy density up to 2000 Wh kg^{-1} with stable cycling, effectively suppressing lithium sulfide dissolution. Silicon (Si) anodes are promising for batteries, but their volume expansion causes short lifetimes. A new Si anode with 70 wt% Si nanoparticles within MXene hollow nanofibers (Si@MHF) delivers high capacity and excellent stability over 200 cycles. Solid-state $Li_2S\|SPE\|Si$ full cells, using this anode and a Li_2S cathode, show high energy density, long cycle life, and remarkable safety, even under abuse conditions.[138] Jiarui He *et al.* present a Li_2S–Co_9S_8/Co cathode for anode-free Li–S batteries that stabilizes Li deposition and mitigates polysulfide shuttling. Co_9S_8/Co electrocatalysts provide nucleation sites for uniform Li_2S distribution and catalyse Li–S redox, enhancing Li_2S utilization. The Li_2S–Co_9S_8/Co cathode achieved 969 mAh g^{-1} initially, maintaining 582 mAh g^{-1} over 100 cycles in anode-free cells. Incorporating tellurium (Te) significantly improved performance, yielding 1025 mAh g^{-1} initially and 865 mAh g^{-1} after 100 cycles (84% retention). Pouch cells delivered 776 mAh g^{-1} at C/20 (4 mg cm^{-2}) Li_2S, 4.5 μL mg^{-1} electrolyte, demonstrating a promising path for practical, low-cost Li–S batteries (Fig. 22).[139]

These collective advancements, particularly in prelithiated Li_2S cathodes and innovative anode-free designs, mark a pivotal moment for solid state lithium–sulfur battery technology and provide a crucial foundation for next-generation energy storage solutions.

2.6. Multifunctional separators for Li–S batteries

Li–S batteries are increasingly recognized as a multifunctional design platform that critically shapes electrochemical performance. Beyond preventing short circuits, separator engineering is now central to addressing the polysulfide shuttle, stabilizing lithium metal, and enabling safety and cycle life improvements.[140]

2.6.1. Separator strategies: from passive barriers to active interfaces. Modern separator design integrates multiple mechanisms.

2.6.1.1. Physical blocking. Ion-selective architectures such as electrospun nanofibers or graphene oxide layers suppress polysulfide transport through tortuous diffusion pathways while maintaining Li^+ conductivity.[141]

2.6.1.2. Chemical adsorption. Polar metal oxides (Al_2O_3, Fe_3O_4, high entropy oxides)[142,143] and heteroatom-doped carbons[6] provide abundant Lewis acid sites that immobilize polysulfides, retaining sulfur within the cathode vicinity.

2.6.1.3. Catalytic conversion. Catalytically active coatings (MoS_2, TiS_2, and MXenes) accelerate polysulfide reduction to insoluble Li_2S, lowering kinetic barriers and minimizing the shuttle duration.[144]

2.6.2. Enabling flexible Li–S batteries: separator advancements. The increasing demand for flexible and wearable electronic devices has intensified the demand for resilient Li–S pouch cells. In these systems, the separator faces amplified demands: it must suppress polysulfides, maintain ionic conductivity, and preserve integrity under repeated bending, twisting, or stretching. Design criteria for flexible separators include (i) mechanical flexibility, (ii) chemical and electrochemical stability, (iii) high ionic transport pathways, and (iv) active polysulfide regulation. Recent breakthroughs

Table 5 Recent advancements in separators for flexible pouch Li–S batteries

	Separator novelty	Performance	Ref.
1	Dual-coated separator combining a solid electrolyte ($LiAlO_2$)	Excellent cycling stability, with only a 0.03% capacity loss per cycle over 500 cycles at a high current of 5C, and a high capacity of 800 mAh g^{-1} even with an ultra-high sulfur loading	145
2	Pore-filling solid electrolyte (PFSE)	The battery demonstrates high performance with a Li-ion conductivity of 0.604 mS cm^{-1}, superior mechanical strength of 200 MPa, and e4xcellent long-term cycling stability, retaining 95% of its initial capacity after 200 cycles	146
3	A polyurethane (PU)-based solid electrolyte (self healing)	Specific capacity of approximately 610 mAh g^{-1} after 125 cycles	147
4	Prussian blue@MXene, and polypropylene	High initial capacity (1042.6 mAh g^{-1}), excellent rate capability (90% capacity retention at 1.0C), and outstanding long-term stability (674.1 mAh g^{-1} after 200 cycles)	148
5	MoS_2/graphene	MoS_2/graphene interlayer delivers an initial discharge capacity of 1642 mAh g^{-1}, and the reversible capacity remains at 720 mAh g^{-1} after 100 cycles	2

highlight multifunctional strategies that reconcile these criteria, transforming separators into mechano-electrochemical regulators as shown in Table 5.

2.6.3. Separators and polymer electrolytes: interfacial synergy. In polymer electrolyte systems, separators play distinct yet complementary roles. For Solid polymer electrolytes (SPEs), the polymer simultaneously acts as a separator and an electrolyte. Here, ionic conductivity and dendrite suppression determine viability, whereas for gel and composite polymer electrolytes (GPEs/CPEs), porous separators act as scaffolds to immobilize hybrid electrolytes. Ceramic-coated membranes enhance thermal stability and polysulfide adsorption, while carbon coatings facilitate electron conduction and redox mediation. This interfacial synergy highlights the evolution of separators from passive membranes to engineered platforms that determine both mechano-electrochemical stability and the translational potential of next-generation Li–S devices.

2.6.4. Performance of flexible pouch cells in solid-state Li–S batteries. The design and fabrication of flexible pouch cells are critical for next-generation wearable and

Table 6 Flexible pouch cell solid state Li–S batteries

Anode	Cathode	Electrolyte	Electrochemical performance	Ref.
Li	S/C	Soft PEO_{10}LiTFSI polymer	Demonstrated 470 Wh kg^{-1} in pouch Li–S batteries, focusing on electrolyte immobilization and polysulfide confinement	149
Li/Cu composite	S/KB	Quasi-solid-state PDOL-$SiCl_4$-DE	Excellent cycling stability with a discharge capacity of 189 mAh after 30 cycles at 0.2C and 167 mAh after 50 cycles at 0.3C (with ~360 mg S loading). Initial open-circuit voltage of 2.176 V	150
50-μm-thick Li laminated on Cu foil (N/P ratio of 2.4)	Carbon black-S (75 wt% S, 4 mg cm^{-2} loading)	Lean electrolyte (2.6 μL mg S^{-1}), implied PEI-IEM-based GPE	Fabricated a 10-Ah-grade pouch cell achieving 412.7 Wh kg^{-1} (based on a 50.45 g cell). Maintained 75% of initial capacity after 30 cycles and exhibited enhanced safety with flame-retardant properties	151
Li (integrated with a solid polymer electrolyte)	SPAN (integrated with a solid polymer electrolyte)	PTMG-HDI-BHDS/LiFSI solution (solid polymer electrolyte – SPE)	Delivered an initial discharge capacity of 602 mAh g $SPAN^{-1}$ at 0.3C. Demonstrated exceptional cycling stability, retaining 560 mAh g $SPAN^{-1}$ with >99% Coulombic efficiency after 700 cycles (93% capacity retention). A high-loading cathode (6.8 mg cm^{-2} SPAN) cell yielded 647 mAh g^{-1} (4.4 mAh cm^{-2} areal capacity) at 0.1C over 110 cycles. Pouch cells maintained 561 mAh g $SPAN^{-1}$ with 91.7% retention after 250 cycles	67
Implied Li-based (All-Solid-State)	Implied sulfur-based (All-Solid-State)	3D MPPL composite solid electrolyte (CSE) with ordered MIL-125–NH2 in PEO-based electrolyte (8.3×10^{-4} S cm^{-1} at 60 °C)	Pouch cells showed robust performance at 60 °C, maintaining 1017.4 mAh g^{-1} at 0.1C for 30 cycles, and >323.2 mAh g^{-1} after 400 cycles at 0.5C. Exhibited notable flexibility and superior safety under destructive conditions, highlighting potential for flexible electronics	152
Li3.75Si	AB@S	LPSCLiIn	Operates at 270 MPa stack pressure with a current density of 1. It provides 1512 mAh g^{-1} capacity within 1–2.6 V, retaining 70.6% after 30 cycles	153
LiIn	CBC@S	PTFE	Requires 500 MPa stack pressure and a current density of 0.15. It delivers 1500 mAh g^{-1} capacity within 1–2.4 V, showcasing exceptional 99% retention after 30 cycles	154
Li	C/S/LGPS-SRm)	LPSCl	Functions at 300 MPa stack pressure with a very low current density of 0.01. It yields 1169 mAh g^{-1} capacity from 1.5–2.8 V, maintaining 81% after 10 cycles	155
Li	S@C	PTFE	Operates at 0.17 current density within 1.5–2.8 V, providing 767 mAh g^{-1} capacity	156
Li	LPSf@LPSCl	LPSCl	Operates at a very low 5–10 kPa stack pressure with 0.21 mA cm^{-2} current density. It delivers 1064 mAh g^{-1} capacity across a broad 0.8–2.4 V range	137

portable electronics. This section explores the electrochemical performance of various flexible pouch cells, showcasing the synergy between their components. Table 5 provides a snapshot of the electrochemical performance of flexible pouch cells using solid-state lithium-sulfur (Li–S) batteries. These systems are highly promising due to their high energy density and potential for flexibility. A soft $PEO_{10}LiTFSI$ polymer electrolyte, for instance, has demonstrated a high gravimetric energy density of 470 Wh kg^{-1}, highlighting its effectiveness in confining polysulfides and improving overall battery performance.[23] Another notable example is the use of poly(tetrafluoroethylene) (PTFE) as a matrix, which, while requiring high stack pressure, delivers an impressive capacity of 1500 mAh g^{-1} and retains 99% of its capacity after 30 cycles at a current density of 0.15 mA cm^{-1}.[28] Table 5 also shows that different anode and cathode materials influence performance. For instance, using LiIn as an anode and CB@S as a cathode yields exceptional capacity retention.[28] Meanwhile, a system with a Li anode and a S@C cathode, using a PTFE electrolyte, provides a capacity of 767 mAh g^{-1}.[30] The use of a composite solid electrolyte (3D MPPL CSE) with a PEO-based electrolyte in an all-solid-state configuration shows robust performance, with a discharge capacity of 1017.4 mAh g^{-1} maintained over 30 cycles and excellent flexibility, making it suitable for modern flexible electronics.[26] These results collectively demonstrate that careful selection and engineering of the polymer electrolyte and other cell components are crucial for achieving high performance, safety, and flexibility in next-generation Li–S batteries. Table 6 shows recent advances in flexible Li–S batteries.

3. Environmental impacts of polymer electrolyte systems

The environmental implications of any technological advancement are pivotal for a sustainable future. Such implications extend beyond greenhouse gas emissions to encompass material toxicity and resource depletion. In comparison to Li-ion batteries, Li–Sulfur batteries exhibit greater environmental sustainability. This is evidenced by their higher environmental characteristic index, which clearly positions them as the cleaner technology[157] (Fig. 23).

Fig. 24a and b illustrate the performance metric scores for ternary batteries. NVP has the highest indicator score (6.63×10^{-7}), while Li–sulfur has the lowest (8.96×10^{-9}). In terms of material vulnerability, the unstable supply of critical raw materials, such as lithium, nickel, and cobalt, significantly impacts the supply chain of battery technologies, which puts environmental risk of Li–S batteries lower in terms of material vulnerability as sulfur is a highly abundant material.[158] Fig. 24c illustrates that the Li–S battery (61.3 kWh) is significantly more environmentally benign than NCM/Graphite (63.8 kWh)[159] with 18.4% less greenhouse gas emission for 320 km. Using

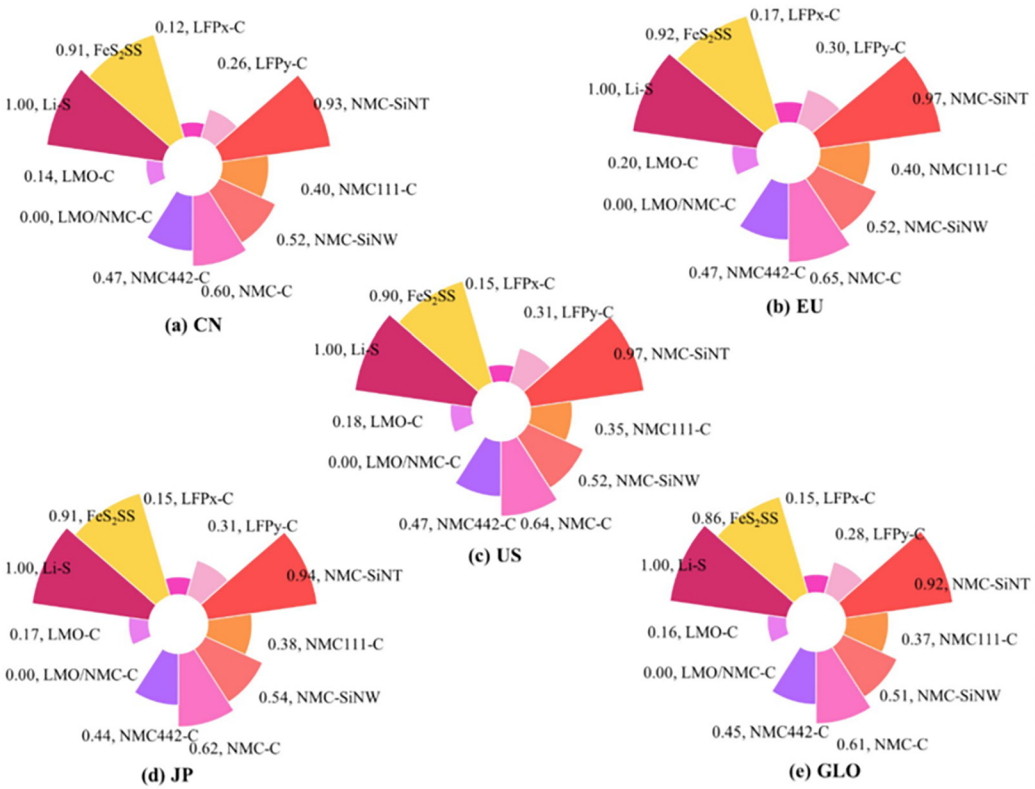

Fig. 23 Environmental characteristic index of different battery technologies in different countries. This figure is reproduced from ref. 157 with permission from Springer Nature copyright 2023.

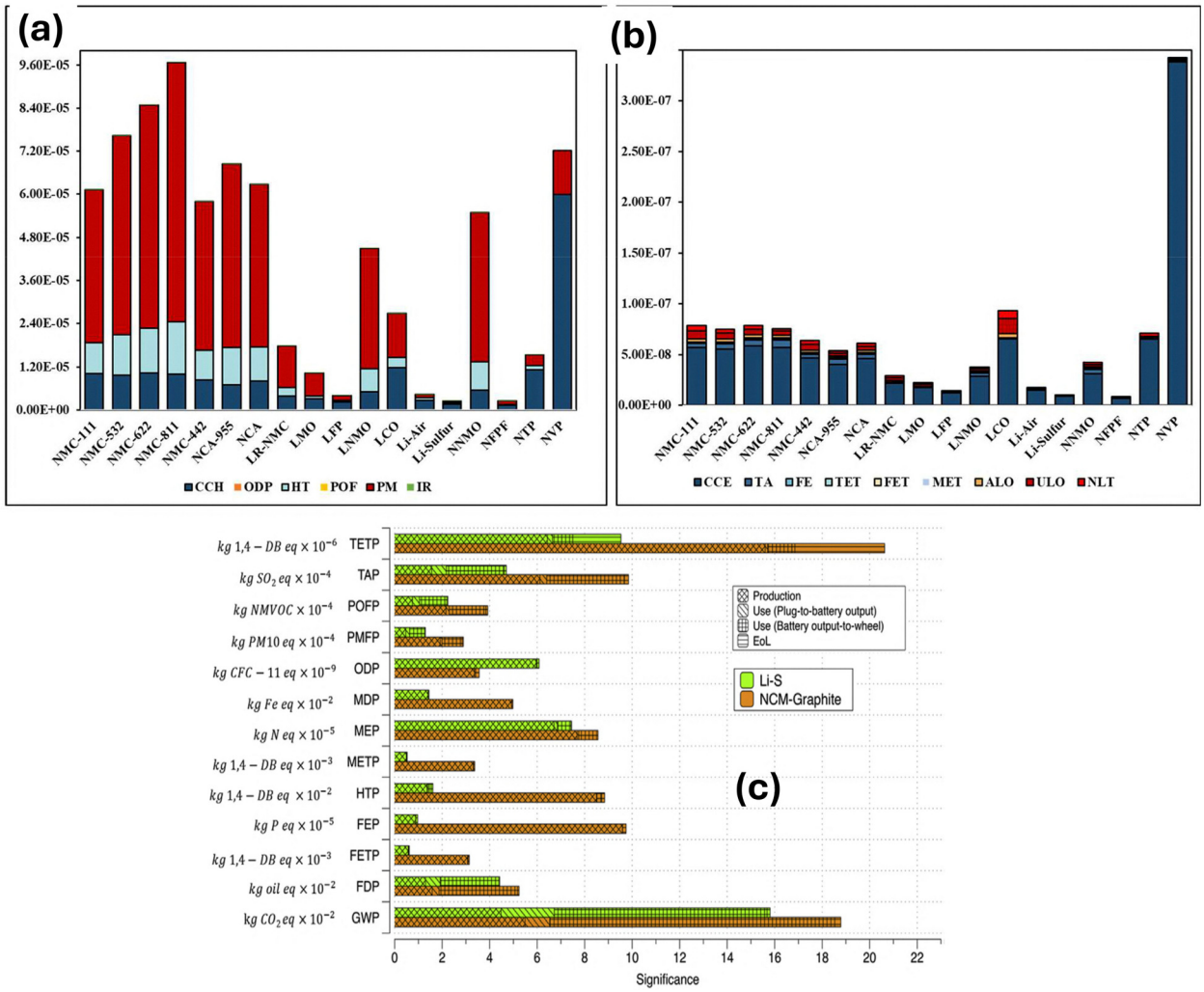

Fig. 24 (a) and (b) Performance metrics and material vulnerability scores for different battery chemistries.[158] This figure is reproduced with permission from Elsevier copyright 2025. (c) Comparison between commercial NCM-G and Li–S for environmental impact parameters.[160] This figure is reproduced from ref with permission from Elsevier copyright 2017.

cradle-to-gate LCA, a GWP of 105 kg CO2e/kWh was reported for a conventional Li–S battery pack.[160] Popien *et al.* estimated the GWP of all-solid-state batteries to range from 80 to 123 kg CO_2e/kWh, for Li–S/NMC622 based battery packs, respectively.[161] Even lower GWP of 52 to 64 kg CO_2e/kWh is reported for all-solid-state Li–S batteries.[162]

Fig. 24a and b illustrate the varying sustainability impacts associated with different polymer electrolytes (PAN, PEO, PPC, PCL, PVDF, and PPL-PPC-PCL). Among these, PAN exhibits the most significant negative environmental effects, while PEO exhibits the least.[163] Additionally, Fig. 24c presents the global warming potential of various solid-state electrolytes, ranging from 0.37 to 10.64 kilograms of CO_2 equivalent per gram of material, significantly lower than those of liquid electrolytes (Fig. 25).

For polymer ceramic electrolytes, in addition to polymer and battery materials the fillers also need to be included for the study of environmental and life cycle analysis in the future, which will also consider the vulnerability and the toxicity potential.

4. Conclusions and future directions for polymer electrolytes

This comprehensive review highlights the profound and accelerating progress in polymer electrolytes for Li–S batteries, driven by sophisticated nanoscale strategies. We have explored types of different polymer electrolytes, their journey from fundamental synthesis to advanced applications, demonstrating their significant advantages over liquid counterparts in safety, thermal and mechanical stability, and sustainability. A decade of dedicated research has advanced various classes of polymer electrolytes—solid, gel, and composite—showcasing their evolving performance metrics, progress and the persistent challenges. This review further underscored their favourable

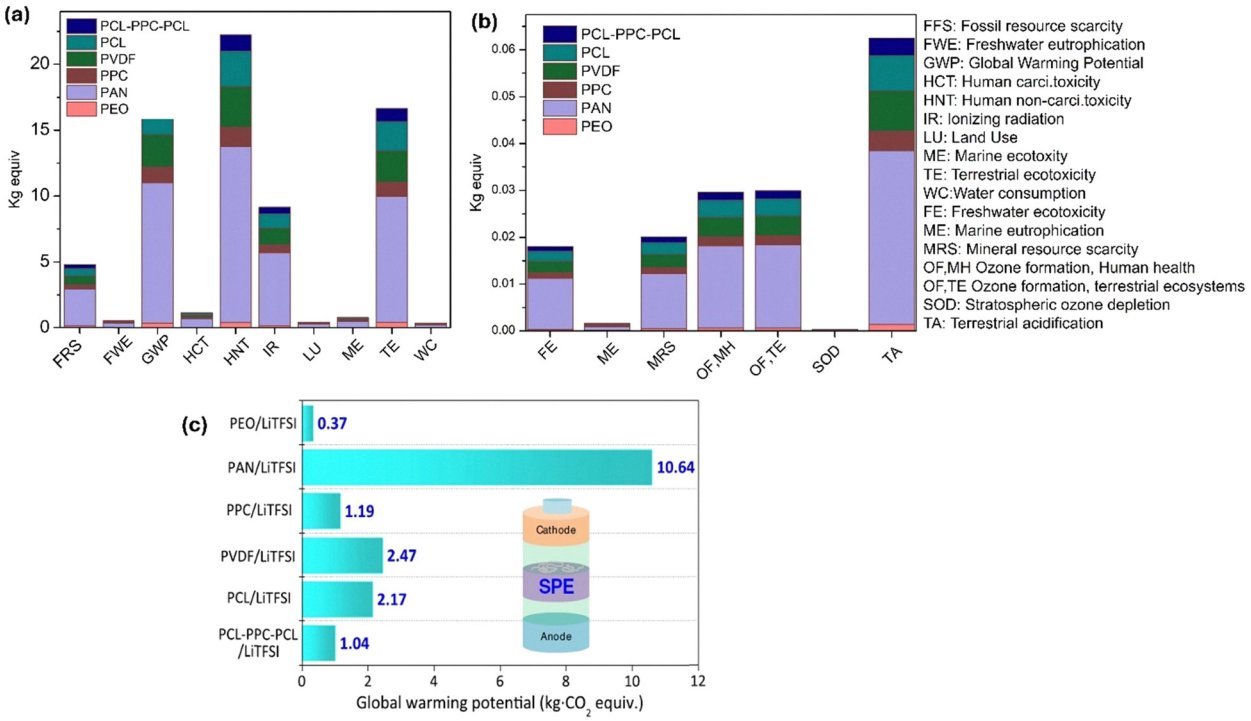

Fig. 25 (a) and (b) Environmental impact parameters for polymer electrolytes. (c) GWP estimation for SPEs. This figure is reproduced from ref. 163 with permission from Wiley copyright 2022.

environmental impact compared to conventional lithium-ion batteries. These advancements stem from the judicious design of highly efficient nanostructured polymer matrices, the strategic incorporation of multi-functional nanofillers, and precision-engineered interfacial techniques. Collectively, these innovations have demonstrably enhanced ionic conductivity, electrochemical stability, and, critically, electrode–electrolyte compatibility, pushing the boundaries of what is achievable. Looking ahead, the burgeoning frontiers of adaptive "smart" electrolytes, capable of responding dynamically to operational conditions, anode free LSBs with Li_2S cathodes and polymer electrolytes, and the powerful integration of machine learning for rational materials design, represent exceptionally promising avenues poised to dramatically accelerate the development and deployment of next-generation polymer electrolytes. However, to fully unleash their potential, future strategies must embrace a multifaceted approach.

4.1. Optimizing self-healing mechanisms and shuttling mitigation

Future research should delve deeper into self-healing triggers (stress, temperature) for targeted design and tailoring the healing properties for specific battery needs.[66,164] This will be coupled with investigations into how these same mechanisms can further suppress lithium polysulfide shuttling, a critical challenge in Li–S batteries.

4.2. Balancing key performance parameters: interfacial stability and ionic conductivity

Development of polymer electrolytes to deliver superior interfacial stability (minimizing resistive layers at the electrode interface) and enhance ionic conductivity for efficient Li-ion transport within the battery demands innovation in electrode–electrolyte design, which includes Li metal–electrolyte interfaces as well as cathode/electrolyte interfaces.

4.3. AI and machine learning: accelerating innovation

4.3.1. Advanced screening of polymer electrolyte components. Machine learning (ML) and artificial intelligence (AI) will be a very critical resource for fast screening vast libraries of polymers, optimizing their suitable combinations for different properties like self-healing, ionic conductivity, interfacial stability, and minimal shuttling behavior, which will help the battery performance synergistically. Even the suitable filler weight percentage salt combination can be determined rapidly through ML.[165] One of the key areas of focus lies in designing advanced materials for Li–S batteries. By leveraging computational tools like high-throughput screening, vast chemical space can be accessed in a fraction of the time, which will help in rapid screening of novel polymer electrolytes with superior properties like ionic conductivity, interfacial compatibility, and mechanical properties. Use of AI and ML will not be limited to material screening, but also used for prediction of battery lifespan, battery state of health prediction, and optimal charge–discharge regime for Li–S battery research.

4.3.2. Predictive modelling and design optimization. By analysing data from simulations and experiments, ML models can predict performance, degradation behaviour, and influence on shuttling, guiding the development of next-generation polymer electrolytes. The vast amount of data generated through computational simulations and experimental testing can be

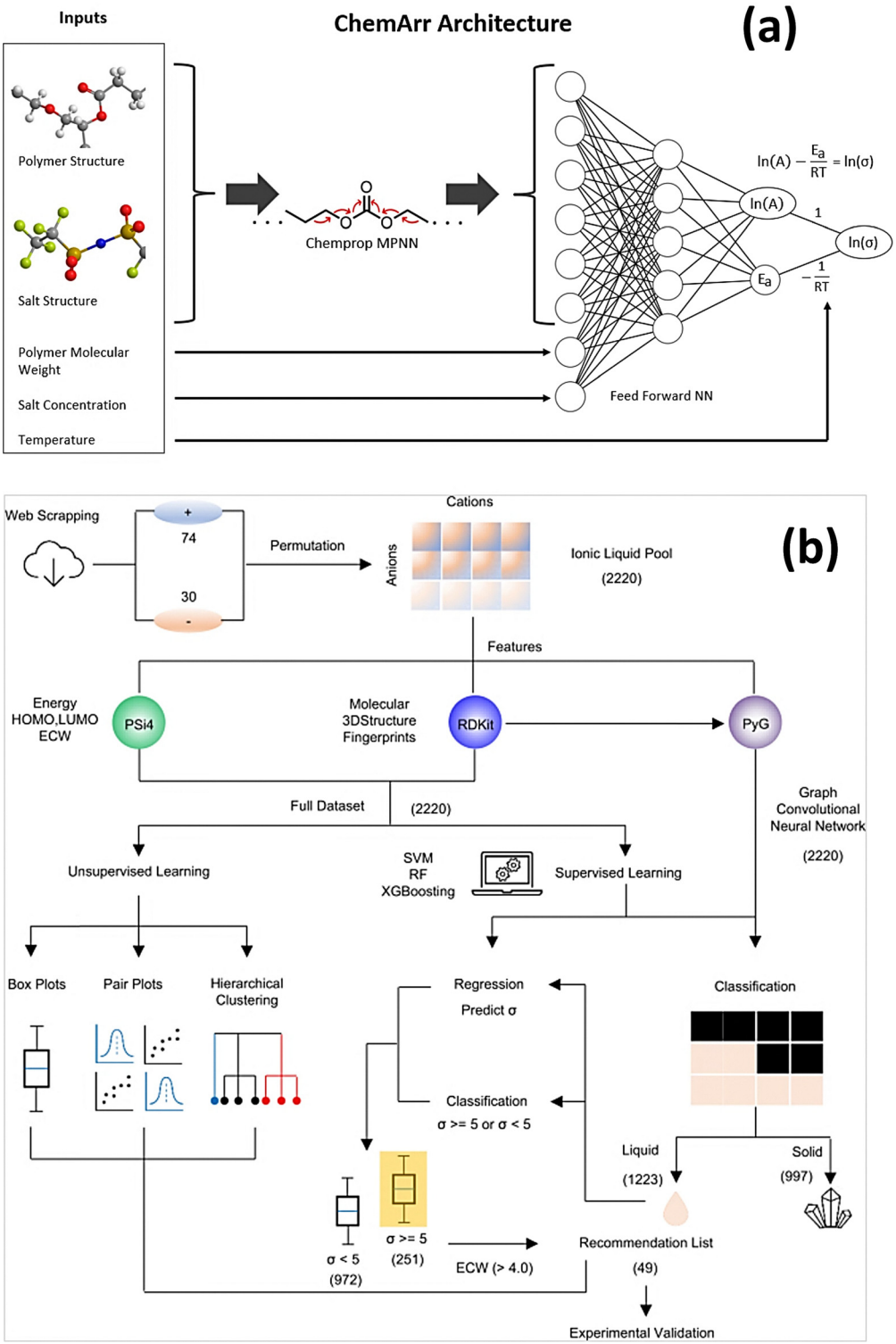

Fig. 26 (a) Diagram of the ChemArr model reproduced from ref. 166, with permission from American Chemical Society copyright 2022. (b) Machine learning workflow for polymer electrolytes from ref. 167 with permission from Springer Nature copyright 2023.

harnessed to train sophisticated ML models. These models can predict the performance of new materials and guide the design of next-generation polymer electrolytes. The future of Li–S battery development lies in a data-driven approach powered by AI and ML. The vast amount of data generated through computational simulations and experimental testing can be used to train sophisticated ML models. These models can then be employed to predict the performance of new materials and guide the design of next-generation polymer electrolytes. Furthermore, these data can be harnessed to develop

intelligent software and hardware that automates battery system design and optimization. ChemArr (MIT),[166] this platform utilizes ML to optimize polymer electrolyte design based on various input parameters. (Fig. 26a). Initiatives like the ''National Institute of Standards and Technology (NIST) Polymer Database Program'' provide publicly accessible data on various polymer properties. Utilization of these data for machine learning input and to streamline the production process should be helpful for researchers working on Li–S battery electrolytes. Wang *et al.* show machine learning guided ionic polymer electrolyte synthesis for lithium batteries for the expert and non-expert users (Fig. 26b) through a neural network,[165] which could be useful for different battery development processes as well as from material manufacturing to battery testing.

4.3.3. *In operando* techniques with intelligence. Real-time observation using advanced in-*operando* characterization techniques will be decisive for understanding critical behaviour of the polymer electrolytes *e.g.* self-healing behaviour, degradation mechanisms, electrolyte–electrode interactions, shuttling phenomenon and other factors that influence shuttling behaviour and overall battery performance. Combining *in situ operando* techniques with ML will allow for real-time characterization of data for battery materials during testing. This will provide insights into degradation mechanisms and will lead to the development of more stable polymer electrolytes. In addition, this will also help in building a dataset for AI for controlling the battery management system adapting the degradation pattern and for determining suitable material parameters and battery testing parameters like charging–discharging rates. This can be helpful in extending battery life and improving safety, as well as accelerating the commercialization.

In summary, polymer based solid electrolytes offer an indispensable and robust pathway toward realizing scalable, safe, and truly sustainable Li–S battery technologies. These materials offer safety due to their inflammability and help to mitigate the ''shuttle effect'', which is the main bottleneck of current Li–S industries. With advancements like self-healing, leveraging AI/ML will accelerate the development. Furthermore, the modification of ionic conductivity and stability using polymer electrolytes will also open avenues in the exploration and development of more materials. It marks a fundamental paradigm shift that is critically aligned with the urgent global imperative for seamless renewable energy integration and the widespread adoption of electrified transportation.

Conflicts of interest

There is no conflict of interest to declare.

Data availability

No primary research results, software or code have been included and no new data were generated or analysed as part of this review.

Acknowledgements

The authors would like to acknowledge the National University of Singapore and CRP and NRF grants.

References

1 J. O'Heir, *Mech. Eng.*, 2017, **139**, 10–11.
2 K. Y. Bae, S. H. Cho, B. H. Kim, B. D. Son and W. Y. Yoon, *Materials*, 2019, **12**(12), 2025.
3 Y. Cui, J. Wan, Y. Ye, K. Liu, L. Y. Chou and Y. Cui, *Nano Lett.*, 2020, **20**, 1686–1692.
4 J. B. Goodenough and K. S. Park, *J. Am. Chem. Soc.*, 2013, **135**, 1167–1176.
5 X. Zeng, M. Li, D. Abd El-Hady, W. Alshitari, A. S. Al-Bogami, J. Lu and K. Amine, *Adv. Energy Mater.*, 2019, **9**, 1–25.
6 M. Zhao, B. Q. Li, X. Q. Zhang, J. Q. Huang and Q. Zhang, *ACS Cent. Sci.*, 2020, **6**, 1095–1104.
7 A. Deshmukh, M. Thripuranthaka, V. Chaturvedi, A. K. Das, V. Shelke and M. V. Shelke, *Prog. Energy*, 2022, **4**, 042001.
8 T. Ould Ely, D. Kamzabek, D. Chakraborty and M. F. Doherty, *ACS Appl. Energy Mater.*, 2018, **1**, 1783–1814.
9 D. Eroglu and J. E. Soc, *J. Electrochem. Soc.*, 2015, **162**, A982.
10 *Battery 2030: Resilient, sustainable, and circular*, **https://www.mckinsey.com/industries/automotive-and-assembly/our-insights/battery-2030-resilient-sustainable-and-circular**.
11 *Reuters, China to invest more than $830min in solid state battery research*, 2024.
12 G. Zhou, H. Chen and Y. Cui, *Nat. Energy*, 2022, **7**, 312–319.
13 Li-S Energy achieves 45% increase in volumetric energy density with new 20-layer semi-solid state lithium sulfur battery.
14 Battery Start-up Theion Unveils Li-S ''Crystal Battery'' for Mobile Applications - Green Car Congress.
15 Lyten Launches Lithium-Sulfur Battery Platform, **https://theevreport.com/lyten-launches-lithium-sulfur-battery-platform**.
16 HARTENERGY, Lyten' s Pilot Plant to Transform Natgas to Lithium-sulfur Batteries, 2023.
17 **https://lyten.com/2025/07/28/lyten-secures-more-than-200-million-in-investment-to-support-its-ongoing-acquisition-strategy/**.
18 Volta Foundation, **https://volta.foundation/battery-report-2024**.
19 G. Bieker, V. Küpers and M. Kolek, *et al.*, *Commun. Mater.*, 2021, **2**, 37.
20 J. He and A. Manthiram, *Energy Storage Mater.*, 2019, **20**, 55–70.
21 A. Manthiram, Y. Fu and Y. S. Su, *Acc. Chem. Res.*, 2013, **46**, 1125–1134.
22 M. Pasta, D. Armstrong, Z. L. Brown, J. Bu, M. R. Castell, P. Chen, A. Cocks, S. A. Corr, E. J. Cussen, E. Darnbrough, V. Deshpande, C. Doerrer, M. S. Dyer, H. El-Shinawi, N. Fleck, P. Grant, G. L. Gregory, C. Grovenor, L. J. Hardwick, J. T. S. Irvine, H. J. Lee, G. Li, E. Liberti, I. McClelland,

C. Monroe, P. D. Nellist, P. R. Shearing, E. Shoko, W. Song, D. S. Jolly, C. I. Thomas, S. J. Turrell, M. Vestli, C. K. Williams, Y. Zhou and P. G. Bruce, *J. Phys Energy*, 2020, **2**(3), 032008.

23 J. Castillo, L. Qiao, A. Santiago, X. Judez, A. S. de Buruaga, G. Jimenez, M. Armand, H. Zhang and C. Li, *Energy Mater.*, 2022, **2**, 200003.

24 E. Quartarone and P. Mustarelli, *Chem. Soc. Rev.*, 2011, **40**, 2525–2540.

25 H. D. Lim, J. H. Park, H. J. Shin, J. Jeong, J. T. Kim, K. W. Nam, H. G. Jung and K. Y. Chung, *Energy Storage Mater.*, 2020, **25**, 224–250.

26 A. Manthiram, X. Yu and S. Wang, Lithium battery chemistries enabled by solid-state electrolytes, *Nat. Rev. Mater.*, 2017, **2**, 16103.

27 Q. Wu, M. Fang, S. Jiao, S. Li, S. Zhang, Z. Shen, S. Mao, J. Mao, J. Zhang, Y. Tan, K. Shen, J. Lv, W. Hu, Y. He and Y. Lu, *Nat. Commun.*, 2023, **14**, 6296.

28 Z. Song, F. Chen, M. Martinez-Ibañez, W. Feng, M. Forsyth, Z. Zhou, M. Armand and H. Zhang, *Nat. Commun.*, 2023, **14**, 4884.

29 K. Li, J. Wang, Y. Song and Y. Wang, *Nat. Commun.*, 2023, **14**, 2789.

30 V. Di Noto, S. Lavina, G. A. Giffin, E. Negro and B. Scrosati, in *Electrochimica Acta*, Elsevier Ltd, 2011, vol. 57, pp. 4–13.

31 J. E. Weston and B. C. H. Steele, *Solid State Ionics*, 1982, **7**(1), 75–79.

32 K. Jeddi, M. Ghaznavi and P. Chen, *J. Mater. Chem. A*, 2013, **1**, 2769–2772.

33 L. Z. Fan, H. He and C. W. Nan, *Nat. Rev. Mater.*, 2021, **6**, 1003–1009.

34 X. Li, S. Liu, J. Shi, M. Huang, Z. Shi, H. Wang and Z. Yan, *Chem. Eng. J.*, 2023, **468**, 143795.

35 Q. Zhao, S. Stalin, C. Z. Zhao and L. A. Archer, *Nat. Rev. Mater.*, 2020, **5**, 229–252.

36 J. Qian, B. Jin, Y. Li, X. Zhan, Y. Hou and Q. Zhang, *J. Energy Chem.*, 2021, **56**, 420–437.

37 J. T. Frith, M. J. Lacey and U. Ulissi, *Nat. Commun.*, 2023, **14**, 420.

38 C. Randall, *SAIC to supply IM Motors EVs with solid-state batteries*, 2024.

39 X. Yu and A. Manthiram, *Energy Storage Mater.*, 2021, **34**, 282–300.

40 D. Dong, B. Zhou, Y. Sun, H. Zhang, G. Zhong, Q. Dong, F. Fu, H. Qian, Z. Lin, D. Lu, Y. Shen, J. Wu, L. Chen and H. Chen, *Nano Lett.*, 2019, **19**, 2343–2349.

41 Y. Su, X. Zhang, C. Du, Y. Luo, J. Chen, J. Yan, D. Zhu, L. Geng, S. Liu, J. Zhao, Y. Li, Z. Rong, Q. Huang, L. Zhang, Y. Tang and J. Huang, *Small*, 2021, **18**(29), 2202069.

42 M. Armand, *Solid State Ion*, 1983, **9–10**, 745–754.

43 B. Zhang, J. Wu, J. Gu, S. Li, T. Yan and X. P. Gao, *ACS Energy Lett.*, 2021, **6**, 537–546.

44 R. Fang, H. Xu, B. Xu, X. Li, Y. Li and J. B. Goodenough, *Adv. Funct. Mater.*, 2021, **31**(2), 2001812.

45 G. Di Donato, T. Ates, H. Adenusi, A. Varzi, M. A. Navarra and S. Passerini, *Batteries Supercaps*, 2022, **5**(7), e202200097.

46 H. Marceau, C. S. Kim, A. Paolella, S. Ladouceur, M. Lagacé, M. Chaker, A. Vijh, A. Guerfi, C. M. Julien, A. Mauger, M. Armand, P. Hovington and K. Zaghib, *J. Power Sources*, 2016, **319**, 247–254.

47 E. Ahiavi, P. Soudant, D. Devaux and R. Bouchet, *Electrochim. Acta*, 2024, **488**, 144202.

48 S. Xue, Y. Liu, Y. Li, D. Teeters, D. W. Crunkleton and S. Wang, *Electrochim. Acta*, 2017, **235**, 122–128.

49 D. Das, A. Chandrasekaran, S. Venkatram and R. Ramprasad, *Chem. Mater.*, 2018, **30**, 8804–8810.

50 Z. Wang, B. Al Alwan, W. Fawaz and K. Y. S. Ng, *J. Electroanal. Chem.*, 2024, **954**, 118017.

51 H. Zhang, C. Liu, L. Zheng, F. Xu, W. Feng, H. Li, X. Huang, M. Armand, J. Nie and Z. Zhou, *Electrochim. Acta*, 2014, **133**, 529–538.

52 G. G. Eshetu, X. Judez, C. Li, M. Martinez-Ibañez, I. Gracia, O. Bondarchuk, J. Carrasco, L. M. Rodriguez-Martinez, H. Zhang and M. Armand, *J. Am. Chem. Soc.*, 2018, **140**, 9921–9933.

53 H. Zhang, U. Oteo, X. Judez, G. G. Eshetu, M. Martinez-Ibañez, J. Carrasco, C. Li and M. Armand, *Joule*, 2019, **3**, 1689–1702.

54 Z. Jia, Y. Liu, H. Li, Y. Xiong, Y. Miao, Z. Liu and F. Ren, *J. Energy Chem.*, 2024, **92**, 548–571.

55 F. Yuan, H. Z. Chen, H. Y. Yang, H. Y. Li and M. Wang, *Mater. Chem. Phys.*, 2005, **89**, 390–394.

56 H. Hua, X. Yang, P. Zhang and J. Zhao, *J. Phys. Chem. C*, 2023, **127**, 17324–17334.

57 Y. Ji, K. Yang, M. Liu, S. Chen, X. Liu, B. Yang, Z. Wang, W. Huang, Z. Song, S. Xue, Y. Fu, L. Yang, T. S. Miller and F. Pan, *Adv. Funct. Mater.*, 2021, **31**(47), 2104830.

58 Z. Ao, Y. Zou, H. Zou, Y. Huang and N. Chen, *Chem*, 2022, **28**(34), e202200543.

59 Z. Ao, Y. Zou, H. Li, N. Chen, Y. Huang and Y. Liang, *Sustainable Mater. Technol.*, 2023, **38**, e00712.

60 V. R. Jeedi, K. K. Ganta, Y. Mallaiah, R. Swarnalatha, S. N. Reddy and A. S. Chary, *J. Polym. Res.*, 2022, **29**, 64.

61 A. Abe, D. Mori, Z. Wang, S. Taminato, Y. Takeda, O. Yamamoto and N. Imanishi, *ChemistryOpen*, 2024, **13**, e202400041.

62 G. Feuillade and P. Perche, *Ion-conductive macromolecular gels and membranes for solid lithium cells*, 1975, vol. 5.

63 S. Skaarup, K. West and B. Zachau-Christiansen, *Solid State Ionics*, 1988, 28–30.

64 L. Chen and L. Z. Fan, *Energy Storage Mater.*, 2018, **15**, 37–45.

65 J. Gao, C. Sun, L. Xu, J. Chen, C. Wang, D. Guo and H. Chen, *J. Power Sources*, 2018, 179–189.

66 S. Wang and M. W. Urban, *Nat. Rev. Mater.*, 2020, **5**, 562–583.

67 F. Pei, L. Wu, Y. Zhang, Y. Liao, Q. Kang, Y. Han, H. Zhang, Y. Shen, H. Xu, Z. Li and Y. Huang, *Nat. Commun.*, 2024, **15**, 351.

68 J. Sheng, Q. Zhang, C. Sun, J. Wang, X. Zhong, B. Chen, C. Li, R. Gao, Z. Han and G. Zhou, *Adv. Funct. Mater.*, 2022, **32**(40), 2203272.

69 T. Zhang, J. Zhang, S. Yang, Y. Li, R. Dong, J. Yuan, Y. Liu, Z. Wu, Y. Song, Y. Zhong, W. Xiang, Y. Chen, B. Zhong and X. Guo, *ACS Appl. Mater. Interfaces*, 2021, **13**, 44497–44508.
70 P. Xie, R. Yang, Y. Zhou, B. Zhang and X. Tian, *Chem. Eng. J.*, 2022, **450**(Part 3), 138195.
71 M. Liu, D. Zhou, Y. B. He, Y. Fu, X. Qin, C. Miao, H. Du, B. Li, Q. H. Yang, Z. Lin, T. S. Zhao and F. Kang, *Nano Energy*, 2016, **22**, 278–289.
72 P.-Q. Wang, W.-W. Shao, L. Zhong, H.-F. Wu, J.-X. Li, M.-Q. Liu, Y. Mei, G. Zhang, H.-X. Liu, X.-Q. Shen and M.-X. Jing, *J. Electrochem. Soc.*, 2023, **170**, 120527.
73 L. L. Chiu and S. H. Chung, *J. Mater. Chem. A*, 2022, **10**, 13719–13726.
74 J. Zheng and Y. Y. Hu, *ACS Appl. Mater. Interfaces*, 2018, **10**, 4113–4120.
75 R. Mukkabla, M. Ojha and M. Deepa, *Electrochim. Acta*, 2020, **334**, 135571.
76 X. Hu, S. R. P. Silva, P. Zhang, K. Liu, S. Zhang and G. Shao, *Chem. Eng. J.*, 2023, **467**, 143378.
77 X. Wang, X. Hao, Y. Xia, Y. Liang, X. Xia and J. Tu, *J. Membr. Sci.*, 2019, **582**, 37–47.
78 D. D. Han, Z. Y. Wang, G. L. Pan and X. P. Gao, *ACS Appl. Mater. Interfaces*, 2019, **11**, 18427–18435.
79 S. Gao, K. Wang, R. Wang, M. Jiang, J. Han, T. Gu, S. Cheng and K. Jiang, *J. Mater. Chem. A*, 2017, **5**, 17889–17895.
80 M. Agostini, D. H. Lim, M. Sadd, C. Fasciani, M. A. Navarra, S. Panero, S. Brutti, A. Matic and B. Scrosati, *ChemSusChem*, 2017, **10**, 3490–3496.
81 M. Rao, X. Geng, X. Li, S. Hu and W. Li, *J. Power Sources*, 2012, **212**, 179–185.
82 W. Li, Y. Pang, T. Zhu, Y. Wang and Y. Xia, *Solid State Ion*, 2018, **318**, 82–87.
83 Y. Q. Shen, F. L. Zeng, X. Y. Zhou, A. Bang Wang, W. Kun Wang, N. Y. Yuan and J. N. Ding, *J. Energy Chem.*, 2020, **48**, 267–276.
84 H. Huang, F. Ding, H. Zhong, H. Li, W. Zhang, X. Liu and Q. Xu, *J. Mater. Chem. A*, 2018, **6**, 9539–9549.
85 S. S. Zhang, D. T. Tran and Z. Zhang, *J. Mater. Chem. A*, 2014, **2**, 18288–18292.
86 K. Jeddi, K. Sarikhani, N. T. Qazvini and P. Chen, *J. Power Sources*, 2014, **245**, 656–662.
87 M. Rao, X. Li, Y. Liao, X. Li and W. Li, *Ionics*, 2015, **21**, 1937–1943.
88 Y. Xia, X. Wang, X. Xia, R. Xu, S. Zhang, J. Wu, Y. Liang, C. Gu and J. Tu, *Chem. – Eur. J.*, 2017, **23**, 15203–15209.
89 Q. Wang, Z. Wen, J. Jin, J. Guo, X. Huang, J. Yang and C. Chen, *Chem. Commun.*, 2016, **52**, 1637–1640.
90 D. Shao, L. Yang, K. Luo, M. Chen, P. Zeng, H. Liu, L. Liu, B. Chang, Z. Luo and X. Wang, *Chem. Eng. J.*, 2020, **389**, 124300.
91 H. M. Wang, Z. Y. Wang, C. Zhou, G. R. Li, S. Liu and X. P. Gao, *Sci. China Mater.*, 2023, **66**, 913–922.
92 D. E. Fenton, M. Parker and P. V. Wright, *Complexes of alkali metal ions with poly(ethylene oxide)*, 1964, vol. 6.
93 Z. Li, H. M. Huang, J. K. Zhu, J. F. Wu, H. Yang, L. Wei and X. Guo, *ACS Appl. Mater. Interfaces*, 2019, **11**, 784–791.
94 M. C. Borghini, M. Mastragostino and S. Passerini, *J. Electrochem. Soc.*, 2003, **150**, A585–A590.
95 L. Hu, Z. Tang and Z. Zhang, *J. Power Sources*, 2007, **166**, 226–232.
96 J. Zheng and Y. Y. Hu, *ACS Appl. Mater. Interfaces*, 2018, **10**, 4113–4120.
97 S. Wang, M. Li, G. Yan, Z. Yang, Y. Guo, X. Sun, Y. Wang, Y. Feng, H. Ding and X. Zhang, *Nanoscale*, 2023, **15**, 12961–12971.
98 J. Zheng and Y. Y. Hu, *ACS Appl. Mater. Interfaces*, 2018, **10**, 4113–4120.
99 Z. Zhang, H. Chen, Z. Hu, S. Zhou, L. Zhang and J. Luo, *Front. Energy*, 2022, **16**, 706–733.
100 K. Sau, S. Takagi, T. Ikeshoji, K. Kisu, R. Sato, E. Campos dos Santos, H. Li, R. Mohtadi and S.-i Orimo, *Commun. Mater.*, 2024, **5**, 122.
101 J. Bae, Y. Li, J. Zhang, X. Zhou, F. Zhao, Y. Shi, J. B. Goodenough and G. Yu, *Angew. Chem.*, 2018, **130**, 2118–2122.
102 J. Li, K. Zhu, Z. Yao, G. Qian, J. Zhang, K. Yan and J. Wang, *Ionics*, 2020, **26**, 1101–1108.
103 H. Kasemägi, H. Kasemägi, M. Klintenberg, M. Klintenberg, A. Aabloo and J. O. Thomas, *J. Mater. Chem.*, 2001, **11**, 3191–3196.
104 P. A. R. D. Jayathilaka, M. A. K. L. Dissanayake, I. Albinsson and B.-E. Mellander, *Effect of nano-porous Al_2O_3 on thermal, dielectric and transport properties of the (PEO) 9 LiTFSI polymer electrolyte system*, 2002.
105 J. Li, F. Xie, W. Pang, Q. Liang, X. Yang and L. Zhang, *Regulate transportation of ions and polysulfides in all-solid-state Li-S batteries using ordered-MOF composite solid electrolyte*, 2024, vol. 10.
106 T. Feng, Y. Hu, L. Xu, J. Huang, S. Hu, L. Zhang and L. Luo, *Mater. Today Energy*, 2022, **28**, 101062.
107 Z. Lei, J. Shen, W. Zhang, Q. Wang, J. Wang, Y. Deng and C. Wang, *Nano Res.*, 2020, **13**, 2259–2267.
108 X. Yin, L. Wang, Y. Kim, N. Ding, J. Kong, D. Safanama, Y. Zheng, J. Xu, D. V. M. Repaka, K. Hippalgaonkar, S. W. Lee, S. Adams and G. W. Zheng, *Adv. Sci.*, 2020, **7**(19), 2001303.
109 S.-M. Liu, M.-X. Chen, Y. Xie, D.-H. Liu, J.-F. Zheng, X. Xiong, H. Jiang, L.-C. Wang, H. Luo and K. Han, *Rare Met.*, 2023, **42**, 2562–2576.
110 P. Sivaraj, K. P. Abhilash, B. Nalini, P. Perumal, K. Somasundaram and P. C. Selvin, *Macromol. Res.*, 2020, **28**, 739–750.
111 H. Cheng, C. Yan, L. Chang, M. Dirican, R. Orenstein and X. Zhang, *ACS Appl. Energy Mater.*, 2024, **7**, 3071–3081.
112 M. Li, J. E. Frerichs, M. Kolek, W. Sun, D. Zhou, C. J. Huang, B. J. Hwang, M. R. Hansen, M. Winter and P. Bieker, *Adv. Funct. Mater.*, 2020, **30**(14), 1910123.
113 F. Chen, P. M. G. Puente, Y. Zhang, S. Cao, X. Lu, Z. Yi, Q. Shen and J. Li, *Solid State Ionics*, 2022, **380**, 115926.
114 Y. Shi, Z. Fan, B. Ding, Z. Li, Q. Lin, S. Chen, H. Dou and X. Zhang, *J. Electroanal. Chem.*, 2021, **881**, 114916.

115 P. Zhai, N. Peng, Z. Sun, W. Wu, W. Kou, G. Cui, K. Zhao and J. Wang, *J. Mater. Chem. A*, 2020, **8**, 23344–23353.
116 M. Li, J. E. Frerichs, M. Kolek, W. Sun, D. Zhou, C. J. Huang, B. J. Hwang, M. R. Hansen, M. Winter and P. Bieker, *Adv. Funct. Mater.*, 2020, **30**(14), 1910123.
117 O. Sheng, C. Jin, J. Luo, H. Yuan, C. Fang, H. Huang, Y. Gan, J. Zhang, Y. Xia, C. Liang, W. Zhang and X. Tao, *J. Mater. Chem. A*, 2017, **5**, 12934–12942.
118 X. Li, D. Wang, H. Wang, H. Yan, Z. Gong and Y. Yang, *ACS Appl. Mater. Interfaces*, 2019, **11**, 22745–22753.
119 X. Zhang, T. Zhang, Y. Shao, H. Cao, Z. Liu, S. Wang and X. Zhang, *ACS Sustainable Chem. Eng.*, 2021, **9**, 5396–5404.
120 S. Bandyopadhyay and B. Nandan, *Mater. Today Energy*, 2023, **31**, 101201.
121 J. Hu, P. He, B. Zhang, B. Wang and L. Z. Fan, *Energy Storage Mater.*, 2020, **26**, 283–289.
122 Z. Wang, J. Sun, R. Liu, Z. Ba, J. Dong, Q. Zhang and X. Zhao, *Small*, 2023, **19**(47), 2303422.
123 L. Gao, J. Li, J. Ju, L. Wang, J. Yan, B. Cheng, W. Kang, N. Deng and Y. Li, *Chem. Eng. J.*, 2020, **389**, 124478.
124 J. Y. Lee, P. H. Chung, S. C. Yeh, T. Y. Yu, W. Y. Lee, N. L. Wu and R. J. Jeng, *J. Phys. Chem. C*, 2021, **125**, 26339–26347.
125 L. Gao, B. Tang, H. Jiang, Z. Xie, J. Wei and Z. Zhou, *Adv. Sustainable Syst.*, 2022, **6**(3), 2100389.
126 L. Gao, J. Li, B. Sarmad, B. Cheng, W. Kang and N. Deng, *Nanoscale*, 2020, **12**, 14279–14289.
127 J. Sheng, Q. Zhang, C. Sun, J. Wang, X. Zhong, B. Chen, C. Li, R. Gao, Z. Han and G. Zhou, *Adv. Funct. Mater.*, 2022, **32**(40), 2203272.
128 S. Bandyopadhyay, A. Gupta, R. Srivastava and B. Nandan, *J. Electroanal. Chem.*, 2023, **945**, 117712.
129 Y. Xia, Q. Wang, Y. Liu, J. Zhang, X. Xia, H. Huang, Y. Gan, X. He, Z. Xiao and W. Zhang, *J. Colloid Interface Sci.*, 2023, **638**, 908–917.
130 M. Xiao, W. Li, M. Yu, B. Lin, D. Peng, Z. Li, S. W. Or, S. Sun and Z. Xing, *Matter*, 2025, **8**(3), 101934.
131 W. Li, Q. Huang, Z. Li, Y. Wang, S. W. Or, S. Sun and Z. Xing, *ACS Energy Lett.*, 2024, **9**(2), 528–537.
132 L. K. J. Ting, Y. Gao, H. Wang, T. Wang, J. Sun and J. Wang, *ACS Omega*, 2022, **7**(45), 40682–40700.
133 L. Yin, W. Li, Q. Cao, S. W. Or and Z. Xing, *Chem*, 2024, **10**(9), 2609–2614.
134 Y. Liu, X. Meng, Z. Wang and J. Qiu, *Chem*, 2024, **10**(9), 2609–2614.
135 H. Jha, I. Buchberger, X. Cui, S. Meini and H. A. Gasteiger, *J. Electrochem. Soc.*, 2015, **162**, A1829–A1835.
136 Z. W. Seh, J. H. Yu, W. Li, P. C. Hsu, H. Wang, Y. Sun, H. Yao, Q. Zhang and Y. Cui, *Nat. Commun.*, 2014, **5**, 5017.
137 Y. Liu, X. Meng, Z. Wang and J. Qiu, *Sci. Adv.*, 2022, **8**, DOI: **10.1126/sciadv.abl8390**.
138 X. Gao, X. Zheng, J. Wang, Z. Zhang, X. Xiao, J. Wan, Y. Ye, L.-Y. Chou, H. K. Lee, J. Wang, R. A. Vilá, Y. Yang, P. Zhang, L.-W. Wang and Y. Cui, *Nano Lett.*, 2020, **20**, 5496–5503.
139 J. He, A. Bhargav and A. Manthiram, *ACS Energy Lett.*, 2022, **7**, 583–590.
140 S. Xia, X. Xu, W. Wu, Y. Chen, L. Liu, G. Wang, L. Fu, Q. Zhang, T. Wang, J. He and Y. Wu, *Mater. Sci. Eng., R*, 2025, **163**, 100924.
141 Y. Z. Liu, Y. Wang, C. W. Wang, J. Y. Wang and J. Z. Wang, *New Carbon Mater.*, 2020, **35**, 1–11.
142 T. Ansari, A. Ghosh, D. Ganguly, B. Muthiah and R. Sundara, *Batteries Supercaps*, 2025, **8**(7), e202400716.
143 A. Chatterjee, D. Ganguly, R. Sundara and S. S. Bhattacharya, *Batteries Supercaps*, 2023, **6**(7), e202300082.
144 P. Guo, D. Liu, Z. Liu, X. Shang, Q. Liu and D. He, *Electrochim. Acta*, 2017, **256**, 28–36.
145 J. Song, S. Xia, N. Wang, J. Peng, B. Peng, W. Wu, L. Liu, X. Yuan, L. Fu, Y. Chen and Y. Wu, *Adv. Mater.*, 2025, **37**(7), e2418295.
146 A. Le Mong, Y. Ahn, R. Puttaswamy and D. Kim, *Energy Mater.*, 2023, **3**, 300035.
147 X. Cui, X. Wang and Q. Pan, *Energy Mater.*, 2023, **3**(4), 300034.
148 G. Wang, J. Li, Z. Du, Z. Ma and G. Shao, *Membranes*, 2022, **12**(2), 134.
149 J. Chen, W. A. Henderson, H. Pan, B. R. Perdue, R. Cao, J. Z. Hu, C. Wan, K. S. Han, K. T. Mueller, J. G. Zhang, Y. Shao and J. Liu, *Nano Lett.*, 2017, **17**, 3061–3067.
150 L. Hu, T. Yang, L. Zhou, X. Yan, Y. Liu, Y. Xia, W. Zhang, J. Zhang, Y. Gan, X. He, X. Xia, R. Fang, X. Tao and H. Huang, *Small*, 2024, **20**(42), 2402862.
151 C. Xing, H. Chen and S. Zhang, *Matter*, 2022, **5**(8), 2523–2525.
152 J. Li, F. Xie, W. Pang, Q. Liang, X. Yang and L. Zhang, *Sci. Adv.*, 2024, **10**(11), DOI: **10.1126/sciadv.adl3925**.
153 Z. Lv, J. Liu, C. Li, J. Peng, C. Zheng, X. Zheng, Y. Wu, M. Xia, H. Zhong, Z. Gong and Y. Yang, *eTransportation*, 2024, **19**, 100298.
154 M. Fiedler, S. Cangaz, F. Hippauf, S. Dörfler, T. Abendroth, H. Althues and S. Kaskel, *Adv. Sustainable Syst.*, 2023, **7**(4), 2200439.
155 H. Yuan, H. X. Nan, C. Z. Zhao, G. L. Zhu, Y. Lu, X. B. Cheng, Q. B. Liu, C. X. He, J. Q. Huang and Q. Zhang, *Batter Supercaps*, 2020, **3**, 596–603.
156 J. K. Hu, H. Yuan, S. J. Yang, Y. Lu, S. Sun, J. Liu, Y. L. Liao, S. Li, C. Z. Zhao and J. Q. Huang, *J. Energy Chem.*, 2022, **71**, 612–618.
157 H. Zhang, B. Xue, S. Li, Y. Yu, X. Li, Z. Chang, H. Wu, Y. Hu, K. Huang, L. Liu, L. Chen and Y. Su, *Sci. Rep.*, 2023, **13**, 7952.
158 Y. Huang, H. Wang and A. Tzachor, *Resour., Conserv. Recycl.*, 2025, **212**, 107978.
159 B. Huang, W. Zhang, J. Chen, Y. Cui, C. Zhu and S. Yan, *J. Electrochem. Soc.*, 2023, **170**, 020506.
160 Y. Deng, J. Li, T. Li, X. Gao and C. Yuan, *J. Power Sources*, 2017, **343**, 284–295.
161 J. L. Popien, C. Thies, A. Barke and T. S. Spengler, *Int. J. Life Cycle Assess.*, 2023, **28**, 462–477.
162 A. Barke, W. Cistjakov, D. Steckermeier, C. Thies, J. L. Popien, P. Michalowski, S. Pinheiro Melo, F. Cerdas,

C. Herrmann, U. Krewer, A. Kwade and T. S. Spengler, *J. Ind. Ecol.*, 2023, **27**, 795–810.
163 A. Larrabide, I. Rey and E. Lizundia, *Adv. Energy Sustainability Res.*, 2022, **3**(10), 2200079.
164 R. Narayan, C. Laberty-Robert, J. Pelta, J. M. Tarascon and R. Dominko, *Adv. Energy Mater.*, 2022, **12**(17), 2102652.
165 K. Li, J. Wang, Y. Song and Y. Wang, *Nat. Commun.*, 2023, **14**, 1895.
166 G. Bradford, J. Lopez, J. Ruza, M. A. Stolberg, R. Osterude, J. A. Johnson, R. Gomez-Bombarelli and Y. Shao-Horn, *ACS Cent. Sci.*, 2023, **9**, 206–216.
167 K. Li, J. Wang, Y. Song and Y. Wang, *Nat. Commun.*, 2023, **14**, 2789.